Center for Aeronautical Research

Bureau of Engineering Research
The University of Texas at Austin
Austin, Texas

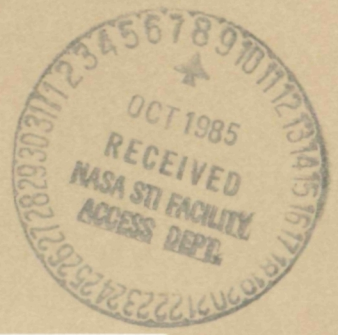

CAR 85-2

A MODAL PARAMETER EXTRACTION PROCEDURE APPLICABLE TO LINEAR TIME-INVARIANT DYNAMIC SYSTEMS

A. J. Kurdila
R. R. Craig, Jr.

NASA Contract NAS8-35338

May 1985

A MODAL PARAMETER EXTRACTION PROCEDURE APPLICABLE TO LINEAR TIME-INVARIANT DYNAMIC SYSTEMS

by

Andrew J. Kurdila *
Roy R. Craig, Jr. +

ASE-EM Department
The University of Texas at Austin
Austin, Texas 78712

* Graduate student, EM
+ Professor, ASE-EM

May 1985

TABLE OF CONTENTS

ACKNOWLEDGMENTS

This work was supported by contract NAS8-35338 of the NASA George C. Marshall Space Flight Center. The authors wish to thank Mr. L. Kiefling for his interest in this work.

Chapter 1

INTRODUCTION

Modal analysis has emerged as a valuable tool in many phases of the engineering design process. Complex vibration and acoustic problems in new designs can often be remedied through use of the method. Moreover, the technique has been used to enhance the conceptual understanding of structures by serving to verify analytical models.

In this thesis, a new modal parameter estimation procedure is presented. The technique is applicable to linear, time-invariant systems and accommodates multiple input excitations. In order to provide a background for the derivation of the method, section (1.1) briefly describes some modal parameter extraction procedures currently in use. Section (1.2) elaborates upon key features implemented in the new technique.

1.1 Extraction Methods

As better experimental measurement procedures and computational resources have become available, a need has likewise developed for more accurate and complete modal surveys. Quite sophisticated modal parameter extraction algorithms have consequently evolved. These methods include time and frequency domain analyses, and differ in the number and types of excitation applied to the structure.

One principal category of extraction techniques recently implemented in modal analysis is based upon representation of the response of a system in terms of characteristic "complex exponentials."

In a general sense, the complex exponential techniques may be considered to include the Ibrahim Time Domain (ITD) method, the Least Squares Complex Exponential (LSCE) method, and the Polyreference method.[1] In the ITD method, the free decay response of a structure is assumed to take the form

$$\underset{\sim}{x}(t) = \sum_{r=1}^{2N} \underset{\sim}{\phi}_r e^{\lambda_r t} \tag{1.1}$$

In Eq. (1.1), $\underset{\sim}{x}(t)$ is the response at N locations on the structure, $\underset{\sim}{\phi}_r$ are modal vectors, and λ_r are the eigenvalues of the system. By collecting the free decay response for several different initial conditions and curve-fitting the collected data to the form in Eq. (1.1), estimates of the modal parameters can be achieved.

In the LSCE method, experimentally derived frequency response functions are fast Fourier transformed to impulse responses in the time domain. Analytically, these impulse responses are assumed to be expressible as

$$h_{ij}(t) = F[H_{ij}(w)] = \sum_{r=1}^{N} [A_{ijr} e^{\lambda_r t} + \bar{A}_{i,r} e^{\bar{\lambda}_r t}] \tag{1.2}$$

where $F[\ ]$ and $(\bar{\ })$ denote Fourier transformation and complex conjugation. The quantities $h_{ij}(t)$, $H_{ij}(w)$ and A_{ijr} in Eq. (1.2) are the impulse response, frequency response function, and rth complex residue for the ith and jth locations on the structure. As in the ITD method, estimates of the modal parameters are achieved by curve-fitting experimental data to the form of the complex exponentials in Eq. (1.2).

Both the LSCE and ITD algorithms have proven capable of generating accurate approximations of modal parameters. Yet, as with any method, criticisms of the approaches have arisen. One potential problem with the ITD method stems from the fact that it utilizes a single input model. Single input refers in this case to the particular initial condition selected in data acquisition. Reference [13] maintains that the ITD method cannot identify repeated modes.

In reference to the LSCE technique, the transformation of frequency response functions back to the time domain may introduce bias errors. Some difficulty has also been noted in determining an estimate of the number of active modes in a particular frequency range. [5]

Unfortunately, the ITD And LSCE methods share an additional common disadvantage. While they both supply a consistent set of natural frequencies, neither approach generates a consistent set of modal vectors. [15] In this context, consistent means a unique set of calculated parameters. The LSCE method, for example, can supply a different set of modal vectors for data acquired using different exciter locations in a single run. [5]

Techniques that generate a consistent set of eigenvalues and eigenvectors have been developed. The Polyreference method, as developed in (20), is one such approach. Two other procedures that calculate consistent parameters are the Direct System Parameter Identification (DSPI) method derived by Leuridan [15] and the Simultaneous Frequency Domain technique of Coppolino. [7] The methods are similar in that they both approximate dynamic system matrices.

The DSPI algorithm is a multiple input, frequency domain parameter extraction technique. The approach may be formulated by transforming the governing equations

$$[M]\ddot{\underset{\sim}{x}}(t) + [c]\dot{\underset{\sim}{x}}(t) + [K]\underset{\sim}{x}(t) = \underset{\sim}{f}(t) \tag{1.3}$$

into their frequency domain form shown in Eq. (1.4).

$$-w^2[M]\underset{\sim}{x}(w) + jw[C]\underset{\sim}{x}(w) + [K]\underset{\sim}{x}(w) = \underset{\sim}{f}(w) \tag{1.4}$$

In Eqs. (1.3) and (1.4), [M], [C] and [K] are N x N mass, damping, and stiffness matrices, respectively. The N-vectors $\underset{\sim}{x}$ and $\underset{\sim}{f}$ represent the response and excitation at N measurement locations on the structure. Because of the DSPI method seeks to estimate directly the entries in [M], [C] and [K], Eq. (1.4) is expanded for discrete frequencies and rearranged into a form suitable for calculation.

$$[T]\underset{\sim}{u} = [V] \tag{1.5}$$

The matrix [T] in Eq. (1.5) is comprised of experimentally collected response, while [V] contains force spectra. The vector $\underset{\sim}{u}$ is composed of the unknown elements in [M], [C] and [K]. By controlling the location that the entries in Eq. (1.4) are indexed into the matrices in Eq. (1.5), constraints such as bandwidth and symmetry may be imposed upon the calculated [M], [C] and [K] matrices. Actual solution of Eq. (1.5) proceeds using a least squares technique. Once the entries in the mass, damping and stiffness matrices are available, a general eigenvalue problem can be assembled and solved for the modal parameters.

While the DSPI method does provide a set of consistent modal parameters, the indexing scheme used in assembling Eq. (1.5) is quite complicated. Even more importantly, if the number of measured responses is large, the DSPI technique requires an inordinate amount of computer space. The method makes no provision for reducing the problem size.

The SFD technique is a single input method that assumes that the response of i "independent" locations on a structure is governed by the set of differential equations

$$[M_i]\ddot{\underset{\sim}{x}}_i(t) + [C_i]\dot{\underset{\sim}{x}}_i(t) + [K_i]\underset{\sim}{x}_i(t) = [D_i]f(t) \qquad (1.6)$$

where

$[M_i]$ = i × i mass matrix

$[C_i]$ = i × i damping matrix

$[K_i]$ = i × i stiffness matrix

$[D_i]$ = i × 1 force distribution matrix

$f(t)$ = a single excitation time history

As is explained shortly, the number of independent coordinates, i, may be considerably less than the total number of measurement locations N. When Eq. (1.6) is Fourier transformed, multiplied by $[M_i]^{-1}$, and rearranged, the fundamental equation of the SFD method emerges

$$\ddot{\underset{\sim}{x}}_i(w) + \left[[\hat{C}_i][\hat{K}_i][\hat{D}_i]\right] \begin{bmatrix} \dot{\underset{\sim}{x}}_i(w) \\ \underset{\sim}{x}_i(w) \\ -f(w) \end{bmatrix} = \underset{\sim}{0} \qquad (1.7)$$

the new matrices $[\hat{C}_i]$, $[\hat{K}_i]$ and $[\hat{D}_i]$ are defined in Eqs. (1.8A), (1.8B), and (1.8C).

$$[\hat{C}_i] = [M_i]^{-1}[C_i] \tag{1.8A}$$

$$[\hat{K}_i] = [M_i]^{-1}[K_i] \tag{1.8B}$$

$$[\hat{D}_i] = [M_i]^{-1}[D_i] \tag{1.8C}$$

If response spectra or frequency response functions are collected, Eq. (1.7) can be expanded for each discrete frequency and solved for the matrices $[\hat{C}_i]$, $[\hat{K}_i]$ and $[\hat{D}_i]$ in a least squares sense. Once these matrices are obtained, a consistent set of eigenvalues and eigenvectors can be calculated from the standard eigenvalue problem

$$\lambda \begin{bmatrix} \dot{x}_i \\ x_i \end{bmatrix} + \begin{bmatrix} [\hat{C}_i] & [\hat{K}_i] \\ [-I] & [0] \end{bmatrix} \begin{bmatrix} \dot{x}_i \\ x_i \end{bmatrix} = \underset{\sim}{0} \tag{1.9}$$

If the number of responses, N, is quite large, the solution of Eq. (1.7) for all measurements, $i = N$, may be cumbersome. The SFD algorithm however, provides a means of reducing the problem size if necessary. In the method, it is possible to choose the i independent locations to be a reasonably sized subset of the total N measurement locations. The remaining $d = N - i$ locations are termed "dependent" coordinates. Solution of Eq. (1.7) using only the independent coordinates is then feasible. Because $i < N$, the eigenvectors calculated in Eq. (1.9) for the reduced problem are of a smaller dimension than full system eigenvectors. The entries of the full eigenvectors corresponding to dependent coordinates are calculated in a least squares sense from

the measured response spectra, or frequency response functions, and the eigenvectors for the independent coordinates.

To better identify closely spaced modes, a version of the SFD algorithm has been derived that utilizes multiple excitation locations. Blair [3] has shown that minor modifications can result in significant improvement in the method's ability to resolve closely spaced modes. Essentially, the single excitation history f(t) in Eq. (1.6) is replaced with an N_p-vector of excitation time histories $\underset{\sim}{f}(t)$, where N_p is the number of exciters. As a result, Eq. (1.7) becomes

$$\ddot{\underset{\sim}{x}}_i(w) + \left[[\hat{C}_i][\hat{K}_i][\hat{D}_i]\right] \begin{bmatrix} \dot{\underset{\sim}{x}}(w) \\ \underset{\sim}{x}(w) \\ -\underset{\sim}{f}(w) \end{bmatrix} = \underset{\sim}{0} \qquad (1.10)$$

where $[\hat{D}_i]$ is now $i \times N_p$. The solution of Eq. (1.10) for the matrices $[\hat{C}_i]$ and $[\hat{K}_i]$, and ultimately the calculation of system eigenvalues and eigenvectors, proceeds identically as in the SFD method.

Selecting the independent coordinates used in model reduction poses a source of difficulty in the SFD technique and Blair's version of the method. In both cases, user judgment is required. In addition, each method uses the normal equations solution procedure, prone to numerical instabilities for poorly conditioned data. As a final point, the theoretical development of the SFD algorithm and Blair's version of the approach assumes that the system damping is proportional, a very limiting restriction.

1.2 Features of the Newly-developed Method

Considering the relative merits of the techniques considered in section (1.1), the approach derived in this thesis is based upon Blair's modification of the SFD algorithm. The current study extends the work of Blair by investigating automatic procedures to reduce the effective problem size. It has been a primary intent of the research to evaluate means of decreasing the user interaction required in generating a reduced-order model. Two reduction strategies are outlined in the thesis.

Furthermore, derivation of the parameter extraction equations proceeds without assumptions regarding the form of damping expected in the physical system. In contrast to the methods of Blair and Coppolino, a theoretical framework is presented that can admit skew-symmetric or non-proportional damping matrices.

Lastly, the technique developed herein utilizes more stable solution procedures than those of Blair and Coppolino. A frequency response function synthesis technique is also described to facilitate modal parameter verification.

The presentation of the new method begins in Chapter 2 with the description of the theoretical basis and computational organization of the technique. A method of verifying the calculated modal parameters is reviewed in Chapter 3. Chapter 4 examines transformations used in reducing large, impractical problems to a reasonable size. Least squares solution procedures and applications to component mode synthesis are topics elaborated upon in Chapters 5 and 6, respectively. Both

analytical and experimental example problems are discussed in Chapter 7. The final chapter of the thesis contains conclusions and recommendations for further work.

Chapter 2

DEVELOPMENT OF THE PARAMETER EXTRACTION METHOD

In developing a modal parameter estimation method for linear, time-invariant dynamic systems, it is assumed that there exists a discrete analytical model, identical to that in Eq. (1.3), that accurately represents the dynamics of the structure.

$$[M]\ddot{\underset{\sim}{x}}(t) + [c]\dot{\underset{\sim}{x}}(t) + [K]\underset{\sim}{x}(t) = \underset{\sim}{f}(t) \tag{2.1}$$

As in Chapter 1, $\ddot{\underset{\sim}{x}}(t)$, $\dot{\underset{\sim}{x}}(t)$ and $\underset{\sim}{x}(t)$ are the acceleration, velocity and displacement time histories at N discrete locations on the structure. Similarly, [M], [C] and [K] are of N × N order and commonly referred to as the mass, damping, and stiffness matrices, respectively. The N-vector $\underset{\sim}{f}(t)$ contains input excitation functions, one for each of the N degrees of freedom.

When dealing with such general systems, it is often more convenient to analyze the set of equations in Eq. (2.1) when they are organized in a different manner. In particular, a state vector formulation is frequently utilized which introduces a 2N-vector of unknowns $\underset{\sim}{X}(t)$.

$$\underset{\sim}{X}(t) = \begin{bmatrix} \dot{\underset{\sim}{x}}(t) \\ \underset{\sim}{x}(t) \end{bmatrix} \tag{2.2}$$

A close inspection of the alternate system

$$[A]\dot{\underset{\sim}{X}}(t) + [B]\underset{\sim}{X}(t) = \underset{\sim}{F}(t) \tag{2.3}$$

where

$$[A] = \begin{bmatrix} [0] & [M] \\ [M] & [C] \end{bmatrix} \tag{2.4}$$

$$[B] = \begin{bmatrix} -[M] & [0] \\ [0] & [K] \end{bmatrix} \tag{2.5}$$

$$F(t) = \begin{bmatrix} 0 \\ \underset{\sim}{f}(t) \end{bmatrix} \tag{2.6}$$

reveals that Eqs. (2.1) and (2.3) are equivalent. The matrices [A] and [B] are of 2N × 2N order, while $\underset{\sim}{F}(t)$ is a 2N-vector.

2.1 Model Reduction

It has been noted in Chapter 1 that some methods are ill-equipped to handle the numerous measurements that can result from practical experimental analyses. An analytical model such as Eqs. (2.1) or (2.3) that is large enough to represent all these experimental degrees of freedom may be difficult, or even impossible, to generate due to limited computer resources. Thus, the need to be able to reduce the size of the dynamic model becomes apparent.

A common method used in analytical dynamics to approximate a large system of differential equations, as in Eq. (2.1), by a smaller system is Ritz analysis. [2, 8] Essentially, the solution $\underset{\sim}{x}(t)$ is approximated by a linear combination of M Ritz basis vectors, $\underset{\sim}{\psi}_i$, such that

$$\underset{\sim}{x}(t) \cong \sum_{i=1}^{M} \gamma_i(t)\underset{\sim}{\psi}_i \tag{2.7}$$

where $M \leq N$. Because the approximation of $\underset{\sim}{x}(t)$ is restricted to the subspace spanned by the Ritz vectors $\underset{\sim}{\psi}_i$, the accuracy of Eq. (2.7) depends upon the Ritz vectors chosen. Reasonable accuracy is achieved only if the Ritz vectors span a significant portion of the "motion space" of the system in Eq. (2.1).

The fact that Ritz analysis can indeed decrease the dimension of a system of equations is apparent when Eq. (2.7) is written in matrix form

$$\underset{\sim}{x}(t) \cong [\underset{\sim}{\psi}_1\ \underset{\sim}{\psi}_2 \cdots \underset{\sim}{\psi}_M]\underset{\sim}{\gamma}(t) = [\underset{\sim}{\psi}_i]\underset{\sim}{\gamma}(t) \tag{2.8}$$

In Eq. (2.8), $[\underset{\sim}{\psi}_i]$ is an N × M matrix, and the original N-vector $\underset{\sim}{x}(t)$ is approximated using a smaller order M-vector $\underset{\sim}{\gamma}(t)$.

Ritz analysis may also be likened to another transformation method encountered in time series analysis. [4] The approach seeks to replace an unwieldy, large set of unknowns by a smaller, statistically similar set. For example, the technique may be applied in signal processing when it is necessary to transmit several signals over a smaller set of channels. To compensate for the limited number of channels, only a subset, or a reduced combination, of the original set are transmitted. The full, original set is then approximated upon reception of the subset of signals. [4]

This process of reducing, and later reconstructing, a set of time histories is embodied in Eqs. (2.9), (2.10A) and (2.10B).

$$\underset{\sim}{\gamma}(t) = [\psi_C]\underset{\sim}{x}(t) \tag{2.9}$$

$$\underset{\sim}{x}(t) \approx [\psi_R]\underset{\sim}{\gamma}(t) \tag{2.10A}$$

$$\underset{\sim}{x}(t) = [\psi_R]\underset{\sim}{\gamma}(t) + \underset{\sim}{\varepsilon}(t) \tag{2.10B}$$

In equation (2.9), the original response N-vector $\underset{\sim}{x}(t)$ is "condensed" via an M × N transformation matrix $[\psi_C]$ to the reduced M-vector $\underset{\sim}{\gamma}(t)$. The condensed vector is assumed more convenient for processing, such as computation or transmission, than the original vector $\underset{\sim}{x}(t)$. When processing of $\underset{\sim}{\gamma}(t)$ is complete, the original N-vector $\underset{\sim}{x}(t)$ may be estimated from the M-vector $\underset{\sim}{\gamma}(t)$ using the N × M matrix $[\psi_R]$ in Eq. (2.10A). Equation (2.10B) simply identifies the error incurred in Eq. (2.10A) as an N-vector $\underset{\sim}{\varepsilon}(t)$. The notation in Eq. (2.10B) is convenient in later discussion of transformation methods.

Comparison of Eqs. (2.8) and (2.10A) reveals that the reconstructing transformation is identical in form to a Ritz analysis transformation. As in the Ritz analysis, the accuracy of Eq. (2.10A) depends upon the selection of $[\psi_C]$ and $[\psi_R]$. This selection process is discussed in Chapter 4.

The above transformations can now be used to produce a reduced-order model. Substituting Eq. (2.10) into Eq. (2.1), and premultiplying by $[\psi_C]$ yields a smaller set of governing equations in the new variable $\underset{\sim}{\gamma}(t)$.

$$[\psi_C][M][\psi_R]\ddot{\underset{\sim}{\gamma}}(t) + [\psi_C][C][\psi_R]\dot{\underset{\sim}{\gamma}}(t) + [\psi_C][K][\psi_R]\underset{\sim}{\gamma}(t) + \begin{matrix}\text{Error}\\ \text{Terms}\end{matrix} = [\psi_C]\underset{\sim}{f}(t) \tag{2.11}$$

Neglecting the error terms and introducing a more compact notation results in the reduced system

$$[M^*]\ddot{\underset{\sim}{\gamma}}(t) + [C^*]\dot{\underset{\sim}{\gamma}}(t) + [K^*]\underset{\sim}{\gamma}(t) \cong [\psi_C]\underset{\sim}{f}(t) \qquad (2.12A)$$

with

$$[M^*] = [\psi_C][M][\psi_R] \qquad (2.12B)$$

$$[C^*] = [\psi_C][C][\psi_R] \qquad (2.12C)$$

$$[K^*] = [\psi_C][K][\psi_R] \qquad (2.12D)$$

where [M*], [C*], and [K*] are M × M mass, damping and stiffness matrices. Because of the omission of error terms, the equality in Eq. (2.12A) is necessarily approximate. However, further equations derived from Eq. (2.12A) are expressed as strict equalities. Lastly, it is worth noting that if $[\psi_C] = [\psi_R]^T$, then [M*], [C*], and [K*] are identical to the matrices obtained in a standard Ritz analysis reduction. [2, 8]

2.2 Frequency Domain Model

With the advent of digital Fourier analyzers, frequency-domain analysis in structural dynamics has flourished. [22] These instruments provide a quick means of generating the frequency spectrum of a time-domain signal and may also directly compute frequency response functions. Because experimental frequency domain data is commonly available and may be easily transformed to represent accelerations, velocities or displacements, a frequency-domain equivalent of the reduced model in Eq.

(2.12) is sought. To this end, it is now necessary to Fourier transform Eq. (2.12).

$$[M^*]\ddot{\underset{\sim}{\gamma}}(w) + [C^*]\dot{\underset{\sim}{\gamma}}(w) + [K^*]\underset{\sim}{\gamma}(w) = [\psi_C]\underset{\sim}{f}(w) \tag{2.13}$$

With [ ] denoting a Fourier transform, the previous notation may be defined

$$\ddot{\underset{\sim}{\gamma}}(w) = F[\ddot{\underset{\sim}{\gamma}}(t)] \tag{2.14A}$$

$$\dot{\underset{\sim}{\gamma}}(w) = F[\dot{\underset{\sim}{\gamma}}(t)] \tag{2.14B}$$

$$\underset{\sim}{\gamma}(w) = F[\underset{\sim}{\gamma}(t)] \tag{2.14C}$$

In practice, experimental acceleration spectra are more prevalent than velocity or displacement spectra. Using the property of Fourier transforms [10], $[f^{(n)}(t)] = (jw)^n f(w)$, Eq. (2.13) can be written in terms of acceleration spectra alone.

$$[M^*]\ddot{\underset{\sim}{\gamma}}(w) + [C^*]\frac{1}{jw}\ddot{\underset{\sim}{\gamma}}(w) + [K^*]\frac{1}{-w^2}\ddot{\underset{\sim}{\gamma}}(w) = [\psi_C]\underset{\sim}{f}(w) \tag{2.15}$$

Normally, a physical system undergoing multi-shaker modal testing has only a few points of excitation and many nodes. In this case, the full N-vector of nodal excitations, $\underset{\sim}{f}(t)$, can be represented by

$$\underset{\sim}{f}(t) = [D]\underset{\sim}{p}(t) \tag{2.16}$$

If N_p is the number of actual exciters, with $N_p << N$, then [D] is an $N \times N_p$ force distribution matrix and $\underset{\sim}{p}(t)$ is an N_p-vector of excitation

functions. When Eq. (2.16) is Fourier-transformed and substituted into Eq. (2.15), a new system results,

$$[M^*]\ddot{\underset{\sim}{\gamma}}(w) + [C^*]\frac{1}{jw}\ddot{\underset{\sim}{\gamma}}(w) + [K^*]\frac{1}{-w^2}\ddot{\underset{\sim}{\gamma}}(w) = [D^*]\underset{\sim}{p}(w) \qquad (2.17)$$

where $[D^*] = [\psi_C][D]$ is an $M \times N_p$ matrix. Premultiplying by $[M^*]^{-1}$ produces the desired reduced-order frequency-domain analytical model for the system described originally by Eq. (2.1).

$$\ddot{\underset{\sim}{\gamma}}(w) + [\hat{C}]\frac{1}{jw}\ddot{\underset{\sim}{\gamma}}(w) + [\hat{K}]\frac{1}{-w^2}\ddot{\underset{\sim}{\gamma}}(w) = [\hat{D}]\underset{\sim}{p}(w) \qquad (2.18)$$

In this expression, $[\hat{D}]$ is an $M \times N$ matrix.

2.3 Organization of Computations

While the transformation scheme outlined in Eqs. (2.9) and (2.10) is defined for continuous, analytic functions, the approach is equally applicable to discrete data. In particular, the contracting transformation $[\psi_C]$ can be used to generate a condensed set of discrete experimental data for the reduced-order model in Eq. (2.18). If $[\underset{\sim}{x}(w_i)]$ represents N_w measured vectors of response spectra,

$$[\underset{\sim}{x}(w_i)] = [\underset{\sim}{x}(w_1)\ \underset{\sim}{x}(w_2)\ \ldots\ \underset{\sim}{x}(w_{N_w})]_{N\times N_w} \qquad (2.19)$$

then a reduced experimental set of spectra may be obtained via a form of Eq. (2.9) expanded for discrete measurements.

$$[\underset{\sim}{\gamma}(w_i)]_{M\times N_w} = [\underset{\sim}{\gamma}(w_1)\ \underset{\sim}{\gamma}(w_2)\ \ldots\ \underset{\sim}{\gamma}(w_{N_w})] = [\psi_C]_{M\times N}[\underset{\sim}{x}(w_i)]_{N\times N_w} \qquad (2.20)$$

A quick inspection of Eqs. (2.9) and (2.10) reveals that results similar to Eqs. (2.19) and (2.20) may be written for the derivatives of $\underset{\sim}{x}(t)$. Thus,

$$\underset{M\times N_w}{[\ddot{\underset{\sim}{\gamma}}(w_i)]} = \underset{M\times N}{[\psi_C]}\underset{N\times N_w}{[\ddot{\underset{\sim}{x}}(w_i)]} \tag{2.21}$$

To accommodate the condensed experimental acceleration spectra obtained in Eq. (2.21), Eq. (2.18) must be expanded and rearranged for N_w discrete frequencies.

$$\underset{M\times(2M+N_p)}{\left[[\hat{C}]\ [\hat{K}]\ [\hat{D}]\right]}\begin{bmatrix}[\frac{1}{jw_i}\ddot{\underset{\sim}{\gamma}}(w_i)]\\ [\frac{1}{-w_i^2}\ddot{\underset{\sim}{\gamma}}(w_i)]\\ [-p(w_i)]\end{bmatrix}_{(2M+N_p)\times N_w} = \underset{M\times N_w}{[-\ddot{\underset{\sim}{\gamma}}(w_i)]} \tag{2.22}$$

Four new matrices are newly defined in Eq. (2.22).

$$[\frac{1}{jw_i}\ddot{\underset{\sim}{\gamma}}(w_i)] = \begin{bmatrix}\frac{1}{jw_1}\ddot{\gamma}_1(w_1) & \cdots & \frac{1}{jw_{N_w}}\ddot{\gamma}_1(w_{N_w})\\ \frac{1}{jw_1}\ddot{\gamma}_2(w_1) & \cdots & \frac{1}{jw_{N_w}}\ddot{\gamma}_2(w_{N_w})\\ \vdots & & \vdots\\ \frac{1}{jw_1}\ddot{\gamma}_M(w_1) & \cdots & \frac{1}{jw_{N_w}}\ddot{\gamma}_M(w_{N_w})\end{bmatrix}_{M\times N_w} \tag{2.23A}$$

$$\left[\frac{1}{-w_i^2}\,\ddot{\underset{\sim}{\gamma}}(w_i)\right] = \begin{bmatrix} -\frac{1}{w_1^2}\ddot{\gamma}_1(w_1) & \cdots & -\frac{1}{w_{N_w}^2}\ddot{\gamma}_1(w_{Nw}) \\ -\frac{1}{w_1^2}\ddot{\gamma}_2(w_1) & \cdots & -\frac{1}{w_{N_w}^2}\ddot{\gamma}_2(w_{N_w}) \\ \vdots & & \vdots \\ -\frac{1}{w_1^2}\ddot{\gamma}_M(w_1) & \cdots & -\frac{1}{w_{N_w}^2}\ddot{\gamma}_M(w_{N_w}) \end{bmatrix}_{M\times N_w} \tag{2.23B}$$

$$\left[\ddot{\underset{\sim}{\gamma}}(w_i)\right] = \begin{bmatrix} \ddot{\gamma}_1(w_1) & \cdots & \ddot{\gamma}_1(w_{N_w}) \\ \ddot{\gamma}_2(w_1) & \cdots & \ddot{\gamma}_2(w_{N_w}) \\ \vdots & & \vdots \\ \ddot{\gamma}_m(w_1) & \cdots & \ddot{\gamma}_m(w_{N_w}) \end{bmatrix}_{M \times N_w} \tag{2.23C}$$

$$\left[-\underset{\sim}{p}(w_i)\right] = \begin{bmatrix} -p_1(w_1) & \cdots & -p_1(w_{N_w}) \\ -p_2(w_1) & \cdots & -p_2(w_{N_w}) \\ \vdots & & \vdots \\ -p_{N_p}(w_1) & \cdots & -p_{N_p}(w_{N_w}) \end{bmatrix}_{N_p \times N_w} \tag{2.23D}$$

If $[\psi_c]$ is given, the only unknown quantities in Eq. (2.22) are the entries in $[\hat{C}]$, $[\hat{K}]$ and $[\hat{D}]$. These matrices implicitly represent the dynamic properties of the reduced physical system. A standard least-squares solution for $[\hat{C}]$, $[\hat{K}]$ and $[\hat{D}]$ may be formulated by transposing and separating the real and imaginary parts of Eq. (2.22).

$$\underset{2N_w \times (2M+N_p)}{\begin{bmatrix} RE\left[\frac{1}{jw_i}\ddot{\underset{\sim}{\gamma}}(w_i)\right]^T & RE\left[\frac{1}{-w_i^2}\ddot{\underset{\sim}{\gamma}}(w_i)\right]^T & RE\left[-\underset{\sim}{p}(w_i)\right]^T \\ IM\left[\frac{1}{jw_i}\ddot{\underset{\sim}{\gamma}}(w_i)\right]^T & IM\left[\frac{1}{-w_i^2}\ddot{\underset{\sim}{\gamma}}(w_i)\right]^T & IM\left[-\underset{\sim}{p}(w_i)\right]^T \end{bmatrix}} \underset{(2M+N_p)\times M}{\begin{bmatrix} [\hat{C}]^T \\ [\hat{K}]^T \\ [\hat{D}]^T \end{bmatrix}} = \underset{2N_w \times M}{\begin{bmatrix} RE\left[-\ddot{\underset{\sim}{\gamma}}(w_i)\right]^T \\ IM\left[-\ddot{\underset{\sim}{\gamma}}(w_i)\right]^T \end{bmatrix}} \tag{2.24}$$

Equation (2.24) may now be solved for $[\hat{C}]$, $[\hat{K}]$ and $[\hat{D}]$ by any one of several methods, two of which are described in Chapter 5.

Because the matrices $[\hat{K}]$, $[\hat{C}]$ and $[\hat{D}]$ are real and constant, the time-domain equivalent of Eq. (2.18) is expressed

$$\ddot{\underset{\sim}{\gamma}}(t) + [\hat{C}]\dot{\underset{\sim}{\gamma}}(t) + [\hat{K}]\underset{\sim}{\gamma}(t) = [\hat{D}]\underset{\sim}{p}(t) \tag{2.25}$$

In a manner analogous to that done for the full system, the state vector formulation for the reduced system in Eq. (2.25) may be written

$$\begin{bmatrix} [I] & [0] \\ [0] & [I] \end{bmatrix} \begin{bmatrix} \ddot{\underset{\sim}{\gamma}}(t) \\ \dot{\underset{\sim}{\gamma}}(t) \end{bmatrix} + \begin{bmatrix} [\hat{C}] & [\hat{K}] \\ [-I] & [0] \end{bmatrix} \begin{bmatrix} \dot{\underset{\sim}{\gamma}}(t) \\ \underset{\sim}{\gamma}(t) \end{bmatrix} = \begin{bmatrix} [\hat{D}]\ p(t) \\ \underset{\sim}{0} \end{bmatrix} \tag{2.26}$$

or more concisely,

$$[\hat{A}]\ \dot{\underset{\sim}{\Gamma}}(t) + [\hat{B}]\ \underset{\sim}{\Gamma}(t) = \hat{\underset{\sim}{F}}(t) \tag{2.27A}$$

where

$$\underset{\sim}{\Gamma}(t) = \begin{bmatrix} \dot{\underset{\sim}{\gamma}}(t) \\ \underset{\sim}{\gamma}(t) \end{bmatrix} \tag{2.27B}$$

Although $[\hat{A}]$ is a 2M × 2M identity matrix, the present notation is retained to simplify discussion of synthesis in Chapter 3.

A standard eigenproblem may be formulated for the eigenvalues and right eigenvectors of Eq. (2.27). If the time dependence of $\underset{\sim}{\Gamma}(t)$ is given by $\underset{\sim}{\Gamma}(t) = \hat{X}e^{\lambda t}$, then the eigenproblem corresponding to Eq. (2.27) can be written

$$\hat{\lambda}_r \underset{\sim}{\hat{X}}_r + [\hat{B}]\underset{\sim}{\hat{X}}_r = \underset{\sim}{0} \tag{2.28}$$

Equation (2.28) introduces a notational convention maintained throughout this thesis. All eigenvectors and static responses in the derivations that follow may be distinguished from other vectors in that they are expressed without an argument denoting time or frequency dependence. From Eq. (2.28), 2M eigenvalues $\hat{\lambda}_r$ and 2M reduced eigenvectors, $\underset{\sim}{\hat{X}}_r$ of length 2M may be extracted. The eigenvalues may be used directly as approximations to the eigenvalues λ_r of the original system (2.3).

The reduced eigenvectors in Eq. (2.28) may be employed to achieve an approximation to the eigenvectors of the full system in Eq. (2.3). Recalling both the form of $\underset{\sim}{X}(t)$ in Eq. (2.2) and the transformation in Eq. (2.10), we have

$$\underset{\sim}{X}(t) = \begin{bmatrix} \dot{\underset{\sim}{x}}(t) \\ \underset{\sim}{x}(t) \end{bmatrix} \tag{2.29}$$

$$\underset{\sim}{x}(t) \cong [\psi_R]\underset{\sim}{\gamma}(t) \tag{2.30}$$

It is immediately apparent that

$$\underset{\sim}{X}(t) \cong \begin{bmatrix} [\psi_R]\dot{\underset{\sim}{\gamma}}(t) \\ [\psi_R]\underset{\sim}{\gamma}(t) \end{bmatrix} = \begin{bmatrix} [\psi_R] & [0\ ] \\ [0\ ] & [\psi_R] \end{bmatrix} \underset{\sim}{\Gamma}(t) \tag{2.31}$$

Equation (2.31) defines the state vector form of the reconstructing $2N \times 2M$ matrix $[\Psi_R]$.

$$\underset{\sim}{X}(t) \cong [\Psi_R]\ \underset{\sim}{\Gamma}(t) \tag{2.32}$$

$$[\Psi_R] = \begin{bmatrix} [\psi_R] & [0\ ] \\ [0\ ] & [\psi_r] \end{bmatrix} \tag{2.33}$$

Finally, the transformation in Eq. (2.32) may be used to approximately reconstruct the full system eigenvectors from the reduced system eigenvectors.

$$\underset{\sim}{X}_r \cong [\Psi_R]\hat{\underset{\sim}{X}}_r \tag{2.34}$$

Chapter 3

FREQUENCY RESPONSE FUNCTION SYNTHESIS

Often in experimental modal analysis, it is necessary to verify that the set of modal parameters obtained is both accurate and complete over the frequency range of interest. A common means of validation is to generate an analytical set of frequency response functions, or FRF's, from the estimated modal parameters. The analytical FRF's may then be visually compared to experimentally collected FRF's. In this manner, spurious modes may be rejected from a set of calculated modal parameters.

3.1 Preliminaries

The derivation of frequency response synthesis formulas has been described in numerous publications. [5, 22, 23] Many synthesis formulas consider the N-dimensional dynamic system of Eq. (2.1)

$$[M]\ddot{\underset{\sim}{x}}(t) + [c]\dot{\underset{\sim}{x}}(t) + [K]\underset{\sim}{x}(t) = \underset{\sim}{f}(t) \tag{3.1}$$

subject to assumptions concerning the form of the damping matrix [C]. Perhaps the most familiar simplification stipulates that the damping matrix may be expressed as a linear combination of [M] and [K]. This proportional damping assumption enables the classical expression for complex frequency response functions $H_{ij}(w)$ to be written [8]

$$H_{ij}(w) = \frac{x_i(w)}{f_j(w)} = \sum_{r=1}^{N} \frac{\underset{\sim}{\phi}_r(i)\underset{\sim}{\phi}_r(j)}{K_r[1 - (\frac{w}{w_r})^2 + j2\xi_r(\frac{w}{w_r})]} \tag{3.2}$$

The N-vectors $\underset{\sim}{\phi}_r$ and parameters w_r are the normal modes and undamped natural frequencies calculated from the eigenvalue problem

$$\{[K] - w_r^2[M]\}\underset{\sim}{\phi}_r = \underset{\sim}{0} \tag{3.3}$$

The scalars K_r and ξ_r are defined in Eqs. (3.4A) and (3.4B).

$$K_r = \underset{\sim}{\phi}_r^T[K]\underset{\sim}{\phi}_r \tag{3.4A}$$

$$\xi_r = \frac{\underset{\sim}{\phi}_r^T[C]\underset{\sim}{\phi}_r}{2\sqrt{K_r M_r}} \tag{3.4B}$$

$$M_r = \underset{\sim}{\phi}_r^T[M]\underset{\sim}{\phi}_r \tag{3.4C}$$

A less restrictive assertion that is frequently encountered maintains that the damping matrix [C] is symmetric. Based on this supposition, reference [20] derives

$$H_{ij}(w) = \frac{x_i(w)}{f_j(w)} = \sum_{r=1}^{2N} \frac{\underset{\sim}{X}_r(j+N)\underset{\sim}{X}_r(i+N)}{a_r(jw - \lambda_r)} \tag{3.5}$$

Equation (3.5) is based upon the state vector form of Eq. (3.1) given in Eqs. (2.3), (2.4), (2.5) and (2.6). The 2N vectors $\underset{\sim}{X}_r$ of length 2N are the right eigenvectors, and the 2N scalars λ_r are the eigenvalues associated with Eq. (2.3), i.e.,

$$\{\lambda_r[A] + [B]\}\underset{\sim}{X}_r = \underset{\sim}{0} \tag{3.6}$$

The parameter a_r is the right eigenvector contraction of the matrix [A].

$$a_r = \underset{\sim}{X}_r^T[A]\underset{\sim}{X}_r \tag{3.7}$$

Using no simplifications regarding the form of the damping matrix [C], references [5] and [23] present a frequency response synthesis formula suitable for general linear, time-invariant systems.

$$H_{ij}(w) = \sum_{r=1}^{2N} \frac{A_{ijr}}{jw - \lambda_r} \tag{3.8}$$

The above representation of $H_{ij}(w)$ stems from the Laplace transform of Eq. (3.1),

$$\{s^2[M] + s[C] + [K]\}\, \underset{\sim}{x}(s) = \underset{\sim}{f}(s) \tag{3.9A}$$

$$\underset{\sim}{x}(s) = \{s^2[M] + s[C] + [K]\}^{-1} \underset{\sim}{f}(s) = [H(s)]\underset{\sim}{f}(s) \tag{3.9B}$$

When a partial fraction expansion is carried out for each term in the matrix [H(s)], the form given in Eq. (3.8) results. For application in this thesis, however, it will be more convenient to represent FRF's for linear, time-invariant systems in terms of an eigenvector expansion similar to Eqs. (3.2) or (3.5).

3.2 Synthesis for Linear, Time-Invariant Systems

A frequency response synthesis formula applicable to general linear, time-invariant systems and expressed in terms of system eigenvectors can be achieved by starting with the state vector form of the governing equations in Eq. (2.3).

$$[A]\dot{\underset{\sim}{X}}(t) + [B]\underset{\sim}{X}(t) = \underset{\sim}{F}(t) \tag{3.10}$$

The right and left eigenproblems associated with Eq. (3.10) are shown in [12] to be

$$\{\lambda_r[A] + [B]\}\underset{\sim}{X}_r = \underset{\sim}{0} \tag{3.11A}$$

$$\{\lambda_r[A]^T + [B]^T\}\underset{\sim}{Y}_r = \underset{\sim}{0} \tag{3.11B}$$

Moreover, it is also proven that these system eigenvectors are bi-orthogonal with respect to the matrices [A] and [B].

$$\underset{\sim}{Y}_j^T[A]\underset{\sim}{X}_i = \begin{cases} a_j & \text{if } j = i \\ 0 & \text{if } j \neq i \end{cases} \tag{3.12A}$$

$$\underset{\sim}{Y}_j^T[B]\underset{\sim}{X}_i = \begin{cases} b_j & \text{if } j = i \\ 0 & \text{if } j \neq i \end{cases} \tag{3.12B}$$

This attribute of $\underset{\sim}{X}_r$ and $\underset{\sim}{Y}_r$ can be used to uncouple the system in Eq. (3.10). The solution $\underset{\sim}{X}(t)$ may be expressed as a superposition of the right eigenvectors.

$$\underset{\sim}{X}(t) = \sum_{r=1}^{2N} \underset{\sim}{X}_r q_r(t) = [\underset{\sim}{X}_r]\underset{\sim}{q}(t) \tag{3.13}$$

The right eigenvectors $\underset{\sim}{X}_r$ comprise the columns of the 2N × 2N matrix $[\underset{\sim}{X}_r]$ and $\underset{\sim}{q}(t)$ is a 2N-vector. When Eq. (3.13) is substituted into Eq. (3.10), and the resulting system is premultiplied by

$$[\underset{\sim}{Y}_r]^T = \begin{bmatrix} \underset{\sim}{Y}_1^T \\ \underset{\sim}{Y}_2^T \\ \cdot \\ \cdot \\ \cdot \\ \underset{\sim}{Y}_N^T \end{bmatrix}, \tag{3.14}$$

Eqs. (3.12A) and (3.12B) assure that the resulting system is diagonalized.

$$[a_r]\dot{q}(t) + [b_r]q(t) = [Y_r]^T F(t) \tag{3.15}$$

When Eq. (3.15) is Fourier transformed, a set of algebraic equations result.

$$\{jw[a_r] + [b_r]\}q(w) = [Y_i]^T F(w) \tag{3.16}$$

Each equation in the 2N rows of Eq. (3.16) may now be solved individually. The kth unknown $q_r(w)$ becomes

$$q_r(w) = \frac{Y^T F(w)}{jwa_r + b_r} \tag{3.17}$$

The original solution $X(w)$ is recovered when Eqs. (3.17) and (3.13) are combined.

$$X(w) = \sum_{r=1}^{2N} \frac{X_r Y_r^T F(w)}{jwa_r + b_r} \tag{3.18}$$

Equation (3.18) assumes a more familiar form when $X(w)$ is expressed in terms of the system eivenvalues λ_r. Premultiplication of the rth right eigenproblem Eq. (3.11A) by the rth left eigenvector generates the identity

$$\lambda_r Y_r^T[A]X_r + Y_r^T[B]X_r = 0 \tag{3.19}$$

or using (3.12A) and (3.12B),

$$\lambda_r a_r + b_r = 0 \tag{3.20}$$

Substitution of Eq. (3.20) into Eq. (3.18) produces a form explicit in the eigenvalues λ_r.

$$\underset{\sim}{X}(w) = \sum_{r=1}^{2N} \frac{\underset{\sim r}{X}\underset{\sim r}{Y}^T \underset{\sim}{F}(w)}{a_r(jw - \lambda_r)} \tag{3.21}$$

The expansion in Eq. (3.21) provides the desired frequency synthesis formula, expressed in terms of eigenvectors, for any linear, time-invariant system. A comparison of Eqs. (3.21) and (3.8) shows that each FRF implied in Eq. (3.21) is given by

$$H_{ij}(w) = \frac{x_i(w)}{f_j(w)} = \sum_{r=1}^{2N} \frac{A_{ijr}}{jw - \lambda_r} \tag{3.22}$$

where the complex residue A_{ijr} is defined in Eq. (3.23).

$$A_{ijr} = \frac{\underset{\sim r}{X}(i+N)\underset{\sim r}{Y}(J+N)}{a_r} \tag{3.23}$$

3.3 Synthesis for the Reduced System

The parameter extraction scheme outlined in Chapter 2 provides approximations for the right eigenvectors $\underset{\sim r}{X}$ and eigenvalues λ_r of the original system. Direct implementation of Eqs. (3.22) and (3.23) would additionally require the estimation of $\underset{\sim r}{Y}$ and a_r. However, frequency response function synthesis can also be accomplished by considering only reduced system parameters.

Following exactly the same steps in section (3.2) for the reduced system model in Eq. (2.27),

$$[\hat{A}]\dot{\hat{\Gamma}}(t) + [\hat{B}]\hat{\Gamma}(t) = \hat{F}(t) \tag{3.24}$$

an identity similar to Eq. (3.21) may be cited for the reduced frequency response

$$\hat{\Gamma}(w) = \sum_{r=1}^{2M} \frac{\hat{X}_r \tilde{Y}_r^T \hat{F}(w)}{\hat{a}_r(jw - \hat{\lambda}_r)} \tag{3.25}$$

The quantities comprising Eq. (3.25) are analogous to those comprising Eq. (3.21), but hold for the reduced system in Eq. (3.24) instead of Eq. (3.10). $\hat{X}_r$, $\hat{Y}_r$, and $\hat{\lambda}_r$ are the right eigenvectors, left eigenvectors, and eigenvalues of the reduced system.

$$\{\hat{\lambda}_r[\hat{A}] + [\hat{B}]\}\hat{X}_r = 0 \tag{3.26A}$$

$$\{\hat{\lambda}_r[\hat{A}]^T + [\hat{B}]^T\}\hat{Y}_r = 0 \tag{3.26B}$$

The scalar $\hat{a}_r$ is the rth left/right eigenvector condensation of the matrix $[\hat{A}]$.

$$\hat{a}_r = \tilde{Y}_r^T[\hat{A}]\hat{X}_r \tag{3.27}$$

Because all of the constituents in Eq. (3.25) can be defined from the parameter extraction procedure in Chapter 2, it can serve as the basis for generating frequency response functions.

Before Eq. (3.25) can be utilized to render a frequency domain solution to the original system of Eq. (2.3), the reconstructing transformation in Eq. (2.32) must be Fourier transformed.

$$\underset{\sim}{X}(w) = \begin{bmatrix} \dot{\underset{\sim}{x}}(w) \\ \underset{\sim}{x}(w) \end{bmatrix} \cong \begin{bmatrix} [\psi_R] & [0] \\ [0] & [\psi_R] \end{bmatrix} \begin{bmatrix} \dot{\underset{\sim}{\gamma}}(w) \\ \underset{\sim}{\gamma}(w) \end{bmatrix} = [\Psi_R] \underset{\sim}{\Gamma}(w) \quad (3.28)$$

Inserting Eq. (3.25) into Eq. (3.28), the full $2N \times 1$ frequency response $\underset{\sim}{X}(w)$ is approximately reconstructed from the reduced $2M \times 1$ response $\underset{\sim}{\Gamma}(w)$.

$$\underset{\sim}{X}(w) \cong [\Psi_R] \sum^{2M} \frac{\hat{\underset{\sim}{X}}_r \tilde{\underset{\sim}{Y}}_r^T \hat{\underset{\sim}{F}}_r(w)}{\hat{a}_r(jw - \hat{\lambda}_r)} \quad (3.29)$$

When the definition of $\hat{\underset{\sim}{F}}(t)$ supplied in Eq. (2.27) is inserted in Eq. (3.29), a relationship among response and excitation spectra emerges.

$$\underset{\sim}{X}(w) \cong [\Psi_R] \sum_{r=1}^{2M} \frac{\hat{\underset{\sim}{X}}_r \tilde{\underset{\sim}{Y}}_r^T \begin{bmatrix} [\hat{D}] \\ [0] \end{bmatrix} \underset{\sim}{p}(w)}{\hat{a}_r(jw - \hat{\lambda}_r)} \quad (3.30A)$$

$$\underset{\sim}{X}(w) \cong [\hat{H}(w)]\underset{\sim}{p}(w) \quad (3.30B)$$

The new $2N \times N_p$ matrix $[\hat{H}(w)]$ may be partitioned into $N \times N_p$ matrices $[\hat{H}_V(w)]$ and $[\hat{H}_D(w)]$ corresponding to the velocity and displacement portions of the vector $\underset{\sim}{X}(w)$.

$$\underset{\sim}{X}(w) = \begin{bmatrix} \dot{\underset{\sim}{x}}(w) \\ \underset{\sim}{x}(w) \end{bmatrix} \cong \begin{bmatrix} [\hat{H}_V(w)] \\ [\hat{H}_D(w)] \end{bmatrix} \underset{\sim}{p}(w) \quad (3.31)$$

If the lower partition associated with the displacement degrees of freedom is extracted from Eq. (3.31), we have

$$\underset{\sim}{x}(w) = [\hat{H}_D(w)]\underset{\sim}{p}(w) \tag{3.32}$$

It is evident that N entries in each of the N_p columns of $[\hat{H}_D(w)]$ approximate the FRF's corresponding to a given exciter location.

Although it would be more desirable to obtain all N × N possible FRF's, instead of only N × N_p, Eq. (3.32) is sufficient for purposes of verification. Currently, digital Fourier analyzers naturally provide FRF's between monitored response and input locations. Thus, at most N × N_p experimental FRF's should be available for validation.

Chapter 4

SELECTION OF TRANSFORMATIONS

It has been noted in section (2.1) that the accuracy achieved in modal parameters for a particular reduced model hinges upon the selection of $[\psi_C]$ and $[\psi_R]$. Two specific reduction techniques are considered in this chapter. Both methods attempt to automate the process of model reduction.

4.1 Independent Coordinate Method

A widely used reduction technique common in both component mode synthesis [8] and experimental modal analysis [3, 7] assumes that a subset of coordinates may be expressed as a linear combination of the remaining coordinates.

$$\underset{\sim}{x}_d(t) = [\psi_{di}]\underset{\sim}{x}_i(t) \tag{4.1}$$

In Eq. (4.1) $\underset{\sim}{x}_d(t)$ is a d-vector of dependent coordinates, $\underset{\sim}{x}_i(t)$ is an i-vector of independent coordinates, and $[\psi_{di}]$ is a d × i matrix. To simplify notation, let $\underset{\sim}{x}_i(t)$ reside in the upper partition of the full, original response N-vector.

$$\underset{\sim}{x}(t) = \begin{bmatrix} \underset{\sim}{x}_i(t) \\ \underset{\sim}{x}_d(t) \end{bmatrix} \tag{4.2}$$

Because it is assumed that only the independent coordinates need be included in the analysis, $\underset{\sim}{x}_i(t)$ may be immediately identified as $\underset{\sim}{y}(t)$ in Eq. (2.9).

$$\underset{\sim}{x}_i(t) \equiv \underset{\sim}{y}(t) = [\psi_C]\underset{\sim}{x}(t) = [\psi_C] \begin{bmatrix} \underset{\sim}{x}_i(t) \\ \underset{\sim}{x}_d(t) \end{bmatrix} \tag{4.3}$$

As a consequence, $[\psi_C]$ in Eq. (4.3) may be written

$$[\psi_C] = \underset{i \times N}{[[I]\ [0]]} \tag{4.4}$$

In Eq. (4.4), [I] is an i × i matrix and [0] is an i × d null matrix.

The reconstructing transformation in equation Eq. (2.10) is also of a particularly simple form. For convenience, recall Eq. (2.10B).

$$\underset{\sim}{x}(t) = [\psi_R]\underset{\sim}{y}(t) + \underset{\sim}{\varepsilon}(t) \tag{4.5}$$

Using Eq. (4.1) and the fact that $\underset{\sim}{y}(t) = \underset{\sim}{x}_i(t)$ produces

$$\begin{bmatrix} \underset{\sim}{x}_i(t) \\ \underset{\sim}{x}_d(t) \end{bmatrix} = \begin{bmatrix} [I] \\ [\psi_{di}] \end{bmatrix} \underset{\sim}{x}_i(t) + \underset{\sim}{\varepsilon}(t) \tag{4.6}$$

Comparing Eqs. (4.5) and (4.6) suggests that

$$[\psi_R] = \begin{bmatrix} [I] \\ [\psi_{di}] \end{bmatrix} \tag{4.7}$$

where [I] is of i × i order.

The only as of yet undefined quantity in $[\psi_C]$ or $[\psi_R]$ is the submatrix $[\psi_{di}]$. This matrix is calculated in a least-squares sense from measured acceleration spectra. By differentiating Eq. (4.1) twice, Fourier-transforming and expanding for N_w discrete frequencies, it is possible to write

$$[\ddot{\underset{\sim}{x}}_d(w_k)] = [\psi_{di}][\ddot{\underset{\sim}{x}}_i(w_k)] \tag{4.8A}$$

where

$$[\ddot{\underset{\sim}{x}}_i(w_k)] = [\ddot{\underset{\sim}{x}}_i(w_1)\ \ddot{\underset{\sim}{x}}_i(w_2)\ \ldots\ \ddot{\underset{\sim}{x}}_i(w_{N_w})]_{i \times N_w} \tag{4.8B}$$

and

$$[\ddot{\underset{\sim}{x}}_d(w_k)] = [\ddot{\underset{\sim}{x}}_d(w_1)\ \ddot{\underset{\sim}{x}}_d(w_2)\ \ldots\ \ddot{\underset{\sim}{x}}_d(w_{N_w})]_{d \times N_w} \tag{4.8C}$$

When Eq. (4.8) is transposed and separated into real and imaginary parts, a standard least-squares formulation emerges for $[\psi_{di}]$.

$$\begin{bmatrix} \mathrm{RE}\left[\ddot{\underset{\sim}{x}}_i(w_k)\right] \\ \mathrm{IM}\left[\ddot{\underset{\sim}{x}}_i(w_k)\right] \end{bmatrix}_{N_w \times i} \begin{bmatrix} \psi_{di} \end{bmatrix}^T_{i \times d} = \begin{bmatrix} \mathrm{RE}\left[\ddot{\underset{\sim}{x}}_d(w_k)\right]^T \\ \mathrm{IM}\left[\ddot{\underset{\sim}{x}}_d(w_k)\right]^T \end{bmatrix}_{N_w \times d} \tag{4.9}$$

Upon solution of Eq. (4.9) for $[\psi_{di}]$, Eqs. (4.4) and (4.7) completely determine the condensing and reconstructing transformations.

While Blair [3] and Coppolino [7] advocate reduction methods employing a subset of the original coordinates, they rely on the judgment of the analyst to select the independent and dependent coordinate groups. However, automatic selection procedures exist. [16] A procedure slightly more rigorous than manual selection is used in this thesis. It performs Gaussian elimination with row and column pivoting to select the dependent coordinate group.

Essentially, the method permutes the rows and columns of the sample spectra matrix

$$[\underset{\sim}{\ddot{x}}(w_1)] = \begin{bmatrix} \ddot{x}_1(w_1) & \cdots & \ddot{x}_1(W_{N_w}) \\ \ddot{x}_2(w_1) & \cdots & \ddot{x}_2(W_{N_w}) \\ \vdots & & \vdots \\ \ddot{x}_N(w_1) & \cdots & \ddot{x}_N(W_{N_w}) \end{bmatrix} \tag{4.10A}$$

as it drives it to the form

$$\begin{bmatrix} x\ x\ x\ x\ x\ x\ x\ x \\ x\ x\ x\ x\ x\ x\ x \\ x\ x\ x\ x\ x\ x \\ x\ x\ x\ x\ x \ \cdots \text{ ETC.} \\ x\ x\ x\ x \\ x\ x\ x \\ x\ x \end{bmatrix} \begin{matrix} \} \text{ i} \\ \\ \\ \\ \} \text{ d} \end{matrix} \tag{4.10B}$$

In so doing, nearly-linearly-dependent rows are driven to the bottom d positions shown in Eq. (4.10B). Row permutation vectors record which of the original rows, or variables, have been shifted to these positions. These variables are selected as the dependent group. This method of selecting the transformations will be referred to as the "independent coordinate method."

When the aforementioned coordinate transformation is utilized, the extraction equations in section (2.3) assume a noteworthy form. Because the generalized, reduced coordinates are simply a subset, $\underset{\sim}{x}_i(t)$, of the original coordinates, Eq. (2.22) may be written

$$\underset{M\times(2M+N_p)}{\left[[\hat{C}]\ [\hat{K}]\ [\hat{D}]\right]}\begin{bmatrix}\left[\frac{1}{jw_i}\ddot{\underset{\sim}{x}}(w_i)\right]\\ \left[\frac{1}{-w_i^2}\ddot{\underset{\sim}{x}}(w_i)\right]\\ [-p(w_i)]\end{bmatrix}_{(2M+N_p)\times N_w} = \underset{M\times N_w}{[-\ddot{\underset{\sim}{\gamma}}(w_i)]} \tag{4.11}$$

The reduced system equation, Eq. (2.27), and eigenvector problem, Eq. (2.28), may also be expressed in terms of a truncated set of the original response degrees of freedom.

$$[\hat{A}]\begin{bmatrix}\ddot{\underset{\sim}{x}}_i(t)\\ \dot{\underset{\sim}{x}}_i(t)\end{bmatrix} + [\hat{B}]\begin{bmatrix}\dot{\underset{\sim}{x}}_i(t)\\ \underset{\sim}{x}_i(t)\end{bmatrix} = \hat{\underset{\sim}{F}}(t) \tag{4.12}$$

$$\hat{\lambda}[\hat{A}]\begin{bmatrix}\dot{\underset{\sim}{x}}_i\\ \underset{\sim}{x}_i\end{bmatrix} + [\hat{B}]\begin{bmatrix}\dot{\underset{\sim}{x}}_i\\ \underset{\sim}{x}_i\end{bmatrix} = \underset{\sim}{0} \tag{4.13}$$

Equations (4.11), (4.12) and (4.13) are precisely those utilized in the method of Blair and Craig. [3]

4.2 Principal Component Method

One distinct advantage of the method outlined in the previous section is that it may be interpreted intuitively. The process of reducing the problem size may be likened to simply picking fewer coordinates. Yet, many mathematically well-defined and robust reduction methods have been developed in the field of statistics.

Principal component analysis is one specific reduction technique suggested in time series analysis literature. Fundamentally,

the procedure seeks to minimize in a statistical sense the error $\underset{\sim}{\varepsilon}(t)$ incurred in the reconstructed signals in Eq. (2.10B).

Once again, development of the method starts with Eqs. (2.9) and (2.10).

$$\underset{\sim}{y}(t) = [\psi_C]\underset{\sim}{x}(t) \tag{4.14}$$

$$\underset{\sim}{x}(t) = [\psi_R]\underset{\sim}{y}(t) + \underset{\sim}{\varepsilon}(t) \tag{4.15}$$

Principal component analysis seeks the transformations $[\psi_C]$ and $[\psi_R]$ such that the expectation of the inner product of the error in Eq. (4.15),

$$E\{\underset{\sim}{\varepsilon}^T(t)\underset{\sim}{\varepsilon}(t)\} \tag{4.16}$$

is minimized. For a zero mean original signal, $E\{\underset{\sim}{x}(t)\} = \underset{\sim}{0}$, the transformations $[\psi_C]$ and $[\psi_R]$ are shown in [4] to be

$$[\psi_C] = \begin{bmatrix} \underset{\sim}{W}_1^T \\ \underset{\sim}{W}_2^T \\ \vdots \\ \underset{\sim}{W}_M^T \end{bmatrix}, \tag{4.17}$$

and

$$[\psi_R] = [\bar{\psi}_C]^T \tag{4.18}$$

The vectors $\underset{\sim}{W}_i$ comprising $[\psi_C]$ and $[\psi_R]$ are the M eigenvectors corresponding to the largest M eigenvalues of the variance matrix for $\underset{\sim}{x}(t)$. The bar over $[\psi_C]$ in Eq. (4.18) denotes conjugation.

In the analysis at hand, complex acceleration spectra are available. If Eqs. (4.14) and (4.15) are differentiated twice, the development of the principal component method outlined in Eqs. (4.16), (4.17) and (4.18) is unchanged. The variance matrix $[S_v]$ for the complex acceleration spectra may be approximated by the product

$$[S_v]_{N\times N} \cong \frac{\overline{[\ddot{\underset{\sim}{x}}(w_1)][\ddot{\underset{\sim}{x}}(w_1)]^T}}{N_w} \tag{4.19}$$

where

$$[\ddot{\underset{\sim}{x}}(w_1)] = [\ddot{\underset{\sim}{x}}(w_1)\ \ddot{\underset{\sim}{x}}(w_2)\ \ldots\ \ddot{\underset{\sim}{x}}(w_{N_w})] \tag{4.20}$$

Because $[S_v]$ is a Hermitian matrix, it has real eigenvalues and complex eigenvectors. Consequently, $[\psi_C]$ and $[\psi_R]$ are complex when formed using principal component analysis. The matrices $[\psi_C]$ and $[\psi_R]$ are now completely defined in Eqs. (4.17), (4.18) and (4.19).

Besides having a sound mathematical basis, principal component analysis has another attractive feature. The error measure expressed in Eq. (4.16) is directly related to the magnitude of the eigenvalues μ_k associated with the eigenvectors not retained in $[\psi_C]$ or $[\psi_R]$.

$$\min E\{\underset{\sim}{\varepsilon}^T(t)\underset{\sim}{\varepsilon}(t)\} = \sum_{k=M+1}^{N} \mu_k \tag{4.21}$$

Equation (4.21) implies that inspecting the eigenvalues of μ_k of the variance matrix of the acceleration spectra can indicate an appropriate order for the reduced model. If a distinct drop in magnitude occurs in the (M + 1)st eigenvalue, then the first M eigenvectors of the variance matrix should be used in $[\psi_C]$ and $[\psi_R]$. This ability to estimate the number of active modes in a frequency range has no parallel in the independent coordinate method.

Chapter 5

SOLUTION OF LEAST SQUARES PROBLEMS

Least-squares analysis is becoming more prevalent in literature dealing with modal parameter identification. The methods of Blair [3], Coppolino [7], and Leuridan [15] are a few examples of new methods that use a least squares, or pseudoinverse, solution procedure. This thesis requires use of the method in two instances: the solution for the reduced system matrices $[\hat{C}]$, $[\hat{K}]$, $[\hat{D}]$ and the definition of $[\psi_{di}]$ in the independent coordinate transformation.

The current chapter describes the essential features of the least-squares solution. A brief background is provided, as well as descriptions of two computational techniques.

5.1 Preliminaries

The need for a least-squares analysis can arise in the solution of the linear set of equations

$$[A]\underset{\sim}{y} = \underset{\sim}{b} \tag{5.1}$$

The coefficient matrix [A] of the above linear system is M × N, the unknown vector $\underset{\sim}{y}$ is N × 1, and $\underset{\sim}{b}$ is M × 1. In perhaps the most common case, and also the problem at hand, there are more equations in Eq. (5.1) than there are unknowns. The overdetermined system, with M > N, generally need not be consistent.

Because an exact solution might not be available, the classical formulation of a least-squares solution seeks to minimize the

L_2 norm of the residual $\underset{\sim}{r} = \underset{\sim}{b} - [A]\underset{\sim}{y}$. As will be seen, the set of vectors, $\{\hat{\underset{\sim}{y}}\}$ that minimize the norm of the residual may contain a single vector, or several vectors, depending upon the specific overdetermined system.

$$\{\hat{\underset{\sim}{y}}\} = \{\underset{\sim}{y} \in \mathbb{R}^N, \underset{\sim}{y} \min \mid [A]\underset{\sim}{y} - \underset{\sim}{b} \mid\} \tag{5.2}$$

There exist other forms of least-squares analysis based on minimization of L_2 and L_∞ norms. [9]

An important trait of least-squares solutions is that the residual $\underset{\sim}{r}$ is orthogonal to the range of [A]. [14] The matrix formulation of this property leads to the normal equations

$$[A]^T(\underset{\sim}{b} - [A]\underset{\sim}{y}) = \underset{\sim}{0} \tag{5.3A}$$

or

$$[A]^T[A]\underset{\sim}{y} = [A]^T\underset{\sim}{b} \tag{5.3B}$$

When [A] is of full column rank, the coefficient matrix $[A]^T[A]$ is positive definite and may be inverted to obtain $\underset{\sim}{y}$ in Eq. (5.3B).

A serious drawback to the normal equations method is that it is not as accurate for a fixed hardware word length as other methods. Its computational cost may be compared to other methods in terms of flops. A flop is the effort required to perform a floating point add, a multiply and some variable indexing. The normal equations method requires about $MN^2/2 + N^3/6$ flops. [9]

In more sophisticated approaches, orthogonal matrices play a central role in the solution for $\{\hat{\underset{\sim}{y}}\}$ in Eq. (5.2). By definition, the inverse of an orthogonal matrix [Q] is its transpose.

$$[Q]^T[Q] = [I] \tag{5.4A}$$

Another useful property of orthogonal matrices is that they preserve Euclidean length. [21]

$$\|[Q]\underset{\sim}{x}\|^2 = ([Q]\underset{\sim}{x})^T[Q]\underset{\sim}{x}) = \underset{\sim}{x}^T[Q]^T[Q]\underset{\sim}{x} = \underset{\sim}{x}^T\underset{\sim}{x} = \|\underset{\sim}{x}\|^2 \tag{5.4B}$$

With this property, the norm in Eq. (5.2) may be replaced by an equivalent norm.

$$\|\underset{\sim}{r}\| = \|[A]\underset{\sim}{y} - \underset{\sim}{b}\| = \|[Q]^T[A]\underset{\sim}{y} - [Q]^T\underset{\sim}{b}\| \tag{5.5}$$

A judicious choice of $[Q]^T$ in Eq. (5.5) can lead to a more simplified expression for the norm $\|\underset{\sim}{r}\|$. One way to characterize the different least squares techniques that follow is by the particular orthogonal matrix $[Q]^T$ they employ.

5.2 Singular Value Decomposition

One possible choice for [Q] in Eq. (5.5) is suggested by the singular value decomposition of [A]. Any M × N matrix [A] may be expressed as the product

$$[A] = [U][\Sigma][V]^T \tag{5.6}$$

where

[U] = an M × M orthogonal matrix

[Σ] = an M × N diagonal matrix

[V] = an N × N orthogonal matrix

The diagonal entries in [Σ], or singular values, are non-negative by definition and may be arranged in a nonincreasing order. Substituting

the singular value decomposition into Eq. (5.5) and choosing $[Q]^T = [U]^T$ yields

$$\|\underset{\sim}{r}\| = \|[\Sigma][V]^T\underset{\sim}{y} - [U]^T\underset{\sim}{b}\| \tag{5.7}$$

A good deal of useful information can be extracted from Eq. (5.7) if the following notations are introduced:

$$[\Sigma] = \begin{bmatrix} \sigma_1 & & & & & \\ & \ddots & & & & \\ & & \sigma_K & & & \\ & & & 0 & & \\ & & & & \ddots & \\ & & & & & 0 \\ & & [0] & & & \end{bmatrix} = \begin{bmatrix} [\sigma_K] & [0] \\ [0] & [0] \end{bmatrix} \tag{5.8A}$$

$$[V]^T\underset{\sim}{y} = \begin{bmatrix} \underset{\sim}{h}_K \\ \underset{\sim}{h}_{N-K} \end{bmatrix} = \underset{\sim}{h} \tag{5.8B}$$

$$[U]^T\underset{\sim}{b} = \begin{bmatrix} \underset{\sim}{g}_K \\ \underset{\sim}{g}_{M-K} \end{bmatrix} = \underset{\sim}{g} \tag{5.8C}$$

Particular attention should be paid to the form of $[\Sigma]$. Only $K \leq N < M$ of the singular values are nonzero, which allows for $N - K$ linearly dependent columns in $[A]$. When Eqs. (5.8A), (5.8B) and (5.8C) are entered into Eq. (5.7), the original norm becomes

$$\|\underset{\sim}{r}\|^2 = \left\| \begin{bmatrix} [\sigma_K] \underset{\sim}{h}_K \\ \underset{\sim}{0} \end{bmatrix} - \begin{bmatrix} \underset{\sim}{g}_K \\ \underset{\sim}{g}_{M-K} \end{bmatrix} \right\|^2 = \left\| \begin{bmatrix} [\sigma_K] \underset{\sim}{h}_K - \underset{\sim}{g}_K \\ \underset{\sim}{g}_{M-K} \end{bmatrix} \right\|^2 \tag{5.9}$$

A straightforward application of the definition of an L_2 norm can simplify Eq. (5.9). If $\underset{\sim}{a}$ is any vector that is partitioned into sub-vectors,

$$\underset{\sim}{a} = \begin{bmatrix} \underset{\sim}{a}_1 \\ \underset{\sim}{a}_2 \end{bmatrix} \qquad \underset{\sim}{a}_1 = \begin{bmatrix} a_1 \\ a_2 \\ \vdots \\ a_{N_1} \end{bmatrix} \qquad \underset{\sim}{a}_2 = \begin{bmatrix} a_{N_1+1} \\ \vdots \\ a_{N_2} \end{bmatrix} \tag{5.10A}$$

then the square of the L_2 norm of $\underset{\sim}{a}$ is given by

$$\|\underset{\sim}{a}\|^2 = (a_1^2 + a_2^2 + \ldots a_{N_2}^2) \tag{5.10B}$$

$$\|a\|^2 = (a_1^2 + a_2^2 + \ldots a_{N_1}^2) + (a_{\substack{N_1+1 \\ 1}}^2 + \ldots a_{N_2}^2) \tag{5.10C}$$

$$\|\underset{\sim}{a}\|^2 = \|\underset{\sim}{a}_1\|^2 + \|\underset{\sim}{a}_2\|^2 \tag{5.10D}$$

When the trivial property shown in Eq. (5.10D) is applied to Eq. (5.9), the norm of the residual may be expressed as a sum.

$$\|\underset{\sim}{r}\|^2 = \|[\ \sigma_K\ ]\underset{\sim}{h}_K - \underset{\sim}{g}_K\|^2 + \|\underset{\sim}{g}_{M-K}\|^2 \tag{5.11}$$

Now, one must carefully consider the rightmost term in Eq. (5.11). The vector $\underset{\sim}{g}_{M-K}$ is defined in Eq. (5.8C) to be the last M - K entries in the product $[U]^T\underset{\sim}{b} = \underset{\sim}{g}$. However, [U] is uniquely defined in the singular value decomposition in Eq. (5.6) and depends solely upon the matrix [A]. Consequently, the product $[U]^T\underset{\sim}{b} = \underset{\sim}{g}$ is fixed for a

given problem, i.e., a given choice of [A] and $\underset{\sim}{b}$. The selection of $\hat{\underset{\sim}{y}}$ has no affect upon $\|\underset{\sim}{g}_{M-K}\|$.

Because $\|\underset{\sim}{g}_{M-K}\|$ is invariant with respect to any solution vector $\hat{\underset{\sim}{y}}$, the condition for minimization of the norm in Eq. (5.11) must be

$$\|[\ \sigma_k\ ]\underset{\sim}{h}_K - \underset{\sim}{g}_K\|^2 = 0 \tag{5.12}$$

From its definition, the norm of a vector is zero if and only if the vector itself is the zero vector

$$[\sim\sigma_k\sim]\underset{\sim}{h}_K - \underset{\sim}{g}_K = \underset{\sim}{0} \tag{5.13A}$$

or

$$[\sim\sigma_k\sim]\underset{\sim}{h}_K = \underset{\sim}{g}_K \tag{5.13B}$$

Combining Eqs. (5.13B) and (5.8B) provides the least-squares solution sought.

$$\hat{\underset{\sim}{y}} = [V]\begin{bmatrix} \underset{\sim}{h}_K \\ \underset{\sim}{h}_{N-K} \end{bmatrix} \tag{5.14A}$$

$$\hat{\underset{\sim}{y}} = \sum_{J=1}^{K} \frac{\underset{\sim}{v}_j \underset{\sim}{u}_j^T \underset{\sim}{b}}{\sigma_j} + \sum_{J=K+1}^{N} \underset{\sim}{v}_j h_j \tag{5.14B}$$

Two important conclusions can be drawn from this analysis. The first holds only when [A] is not of full column rank, or $K < N$. In this case, the choice of $\underset{\sim}{h}_{N-K}$ in Eq. (5.14) has no effect upon $\|\underset{\sim}{r}\|$ in Eq. (5.9). As a result, $\hat{\underset{\sim}{y}}$ in Eq. (5.14B) is not unique. Any choice of $\underset{\sim}{h}_{N-K}$ results in the same residual $\|r\|$. In practice, $\underset{\sim}{h}_{N-K}$ is set equal to $\underset{\sim}{0}$.

The second conclusion pertains when [A] is of full column rank, or K = N. In this event, $\underset{\sim}{h}_{N-K}$ does not exist. No ambiguity then remains in Eq. (5.14B). The least-square solution $\hat{\underset{\sim}{y}}$ is unique.

Equation (5.14B) defines the least squares solution explicitly in terms of the matrices obtained in a singular value decomposition of [A]. The actual numerical technique that produces the decomposition is quite lengthy. It involves application of several transformations to drive [A] to bidiagonal form, then uses an iterative technique to achieve the final diagonal singular values. A more efficient form of singular value decomposition for solving least squares problems does not form [U] and $[V]^T$ explicitly. It requires approximately $2MN^2 + 4N^3$ flops. [9]

5.3 Householder Transformations

If it is known beforehand that [A] is of full column rank, Householder's method may be used instead of a computationally expensive singular value decomposition. In Householder's method, the norm

$$\|\underset{\sim}{r}\| = \|[Q]^T[A]\underset{\sim}{y} - [Q]^T\underset{\sim}{b}\| \tag{5.15}$$

is simplified by choosing [Q] to be defined from the QR decomposition of [A].

$$[A] = [Q][R] \tag{5.16}$$

In Eq. (5.16), [Q] is an M × M orthogonal matrix and [R] is an M × N upper triangular matrix.

$$[R] = \begin{bmatrix} x & x & x & x & x & x & x \\ & x & x & x & x & x & x \\ & & x & x & x & x & x \\ & & & x & x & x & x \\ & & & & x & x & x \\ & & & & & x & x \\ & & & & & & x \\ & & & [0] & & & \end{bmatrix} = \begin{bmatrix} [R_u] \\ [0] \end{bmatrix} \tag{5.17}$$

All M × N matrices [A] may be factored as shown in Eqs. (5.16) and (5.17). The matrix $[R_u]$ is the M × M upper triangular part of [R]. The assumption that [A] is of full column rank insures that none of the pivot values, or diagonal entries, of $[R_u]$ are zero.

Substitution of (5.16) into (5.15) and introduction of the notation

$$[Q]^T \underset{\sim}{b} = \begin{bmatrix} \underset{\sim}{g}_N \\ \underset{\sim}{g}_{M-N} \end{bmatrix} \tag{5.18}$$

generates a norm quite similar to that encountered in section (5.2).

$$\|\underset{\sim}{r}\|^2 = \left\| \begin{bmatrix} [R_u]\underset{\sim}{y} \\ \underset{\sim}{0} \end{bmatrix} - \begin{bmatrix} \underset{\sim}{g}_N \\ \underset{\sim}{g}_{M-N} \end{bmatrix} \right\|^2 = \left\| \begin{bmatrix} [R_u]\underset{\sim}{y} - \underset{\sim}{g}_N \\ \underset{\sim}{g}_{M-N} \end{bmatrix} \right\|^2 \tag{5.19}$$

$$\|\underset{\sim}{r}\|^2 = \|[R_u]\underset{\sim}{y} - \underset{\sim}{g}_N\|^2 + \|\underset{\sim}{g}_{M-N}\|^2 \tag{5.20}$$

Following the same reasoning used in section (5.2), the condition for minimization of the norm in Eqs. (5.19) and (5.20) is seen to be

$$[R_u]\underset{\sim}{y} = \underset{\sim}{g}_N \tag{5.21}$$

Solution of Eq. (5.21) is particularly easy as it corresponds to the backsubstitution phase of an LU factorization. Equations (5.16),

(5.18) and (5.21) completely determine the solution of a least-squares problem via the Householder method. Because the matrix [A] is assumed to be full rank, the solution in Eq. (5.21) is always unique.

The factorization in Eq. (5.16) is never carried out explicitly. Instead, a sequence of Householder transformations, $[Q_i]^T$, are applied to [A] to drive it to upper triangular form. A Householder transformation is any matrix of the form

$$[Q_i]^T = [I] - 2\underset{\sim}{V}^T\underset{\sim}{V} \tag{5.22}$$

where $\underset{\sim}{V}^T\underset{\sim}{V} = 1$. Matrices of this type have the property that given any two vectors $\underset{\sim}{x}$ and $\underset{\sim}{y}$ of equal length, a matrix $[Q_i]^T$ can be found such that

$$[Q_i]^T\underset{\sim}{x} = \underset{\sim}{y} \tag{5.23}$$

The desired $[Q_i]^T$ is calculated using (5.22) and

$$\underset{\sim}{V} = (\underset{\sim}{x} - \underset{\sim}{y})/\|\underset{\sim}{x} - \underset{\sim}{y}\| \tag{5.24}$$

The diagonalization of [A] is achieved by applying a Householder transformation to [A] and $\underset{\sim}{b}$ for each of the N columns of [A]. In the first transformation, $\underset{\sim}{x}$ is chosen to be the first column of [A] and $\underset{\sim}{y}$ is selected to be

$$\underset{\sim}{y} = \begin{bmatrix} 1 \\ 0 \\ 0 \\ \cdot \\ \cdot \\ \cdot \end{bmatrix} \tag{5.25}$$

When $[Q_1]^T$ corresponding to the above choice of $\underset{\sim}{x}$ and $\underset{\sim}{y}$ is applied to [A] and $\underset{\sim}{b}$, the first column of [A] is put in upper diagonal form. In the Kth subsequent step, $\underset{\sim}{x}$ is chosen to be the Kth column of [A], and $\underset{\sim}{y}$ is selected to be

$$\underset{\sim}{y} = \begin{bmatrix} a_{1,K} \\ \vdots \\ a_{K-1,K} \\ \pm\left(|a_K|^2 - \sum_{i=1}^{K-1} a_{iK}^2\right)^{\frac{1}{2}} \\ 0 \\ \vdots \\ 0 \end{bmatrix} \tag{5.26}$$

Application of $[Q_1]^T$, calculated from the above $\underset{\sim}{x}$ and $\underset{\sim}{y}$, to [A] and $\underset{\sim}{b}$ puts the Kth column of [A] in upper triangular form, while leaving the previous K - 1 columns unchanged. The entire product of individual transformations form the matrix $[Q]^T$ in Eq. (5.15).

$$\underbrace{([Q_N]^T[Q_{N-1}]^T \cdots [Q_1]^T)}_{[Q]^T}[A] = [R] \tag{5.27}$$

The computational cost of a Householder solution of the least squares problem is significantly less than that of singular value decomposition. The flop count for Householder orthogonalization is $MN^2 - \frac{1}{3}N^3$. Both singular value decomposition and Householder orthogonalization are of comparable stability and yield roughly twice as many precise digits for a given hardware word length as the normal equations method. [14]

Chapter 6

APPLICATIONS TO COMPONENT MODE SYNTHESIS

6.1 Preliminaries

Often in computational dynamics, it is necessary to achieve a solution to the analytical model in Eq. (2.1) for a system that has many degrees of freedom N.

$$[M]\ddot{\underset{\sim}{x}}(t) + [c]\dot{\underset{\sim}{x}}(t) + [K]\underset{\sim}{x}(t) = \underset{\sim}{f}(t) \qquad (6.1)$$

One class of solution technique applicable to Eq. (6.1) involves integration of the set of equations in a time-stepping procedure [2, 8]. However, the direct integration of Eq. (6.1) for very large N can be computationally expensive.

An alternative to integration of the full system of equations in Eq. (6.1) is the component mode synthesis method. In addition to extremely large problems, this approach is also well suited to systems composed of a set of natural components. In the technique, the full system is first subdivided into substructures. Each component then undergoes a dynamic analysis to determine its "component modes."

Originally, component modes were simply the free vibration mode shapes of the substructure, calculated with the component boundaries to other components either fixed or free. In current variants of component mode synthesis, the component modes have come to include other fundamental component shapes. The deformation pattern associated with a unit static displacement is known as a constraint mode, while that shape

resulting from a unit statically applied force is known as an attachment mode.

The final step in component mode synthesis involves using a reduced number of the component modes as Ritz vectors in a reduction scheme similar to Eq. (2.9). A reduced order system model is assembled and solved using the Ritz approximations for each component.

In reference [24], Rubin insists that the most worthwhile component mode synthesis techniques should make possible the incorporation of experimental substructure test results. The experimental parameter extraction scheme developed in this thesis can complement the component mode synthesis methods described in Howsman [12] or Chung [6]. These particular techniques employ free-interface modes of vibration and a form of attachment modes as substructure Ritz vectors.

The remainder of Chapter 6 describes how the present formulation of parameter extraction can be used to obtain experimental component modes to supplement, replace or simply verify analytically-determined free interface mode shapes and attachment modes. Section 6.2 briefly outlines the component mode synthesis procedure of Howsman [12], while section 6.3 describes the analytic formulation of the substructure Ritz vectors. The calculation of the appropriate Ritz vectors from experimental data is summarized in section 6.4.

6.2 Component Mode Synthesis for Linear, Time-Invariant Systems

If the system of Eq. (6.1) is comprised of two subsystems, the dynamics of each component may be represented in the form

$$[M_\alpha]\ddot{\underset{\sim}{x}}_\alpha(t) + [C_\alpha]\dot{\underset{\sim}{x}}_\alpha(t) + [K_\alpha]\underset{\sim}{x}_\alpha(t) = \underset{\sim}{f}_\alpha(t) \qquad (6.2A)$$

$$[M_\beta]\ddot{\underset{\sim}{x}}_\beta(t) + [C_\beta]\dot{\underset{\sim}{x}}_\beta(t) + [K_\beta]\underset{\sim}{x}_\beta(t) = \underset{\sim}{f}_\beta(t) \qquad (6.2B)$$

where the α-matrices are of $N_\alpha \times N_\alpha$ and the β-matrices are of order $N_\beta \times N_\beta$. Generally, the component mass, damping and stiffness matrices are obtained analytically, perhaps using finite element analysis. Although only two components, α and β, are described above, extension of the following procedure to an arbitrary number of substructures is straightforward. In keeping with the philosophy of accommodating the most general structures, Eqs. (6.2A) and (6.2B) may also be written using a state vector formulation

$$[A_\alpha]\dot{\underset{\sim}{X}}_\alpha(t) + [B_\alpha]\underset{\sim}{X}_\alpha(t) = \underset{\sim}{F}_\alpha(t) \qquad (6.3A)$$

$$[A_\beta]\dot{\underset{\sim}{X}}_\beta(t) + [B_\beta]\underset{\sim}{X}_\beta(t) = \underset{\sim}{F}_\beta(t) \qquad (6.3B)$$

$\underset{\sim}{X}_\alpha(t)$ and $\underset{\sim}{X}_\beta(t)$ are of length $2N_\alpha$ and $2N_\beta$, respectively. The state formulation matrices $[A_\alpha]$ and $[B_\alpha]$ are of $2N_\alpha \times 2N_\alpha$ order and partitioned as

$$[A_\alpha] = \begin{bmatrix} [0] & [M_\alpha] \\ [M_\alpha] & [C_\alpha] \end{bmatrix} \qquad (6.4A)$$

and

$$[B_\alpha] = \begin{bmatrix} -[M_\alpha] & [0] \\ [0] & [K_\alpha] \end{bmatrix} \qquad (6.4B)$$

The $2N_\beta \times 2N_\beta$ matrices $[A_\beta]$ and $[B_\beta]$ are similarly organized.

The components in Eqs. (6.2A) and (6.2B) must be coupled together to insure that they act as a system. Conceptually, this condition is equivalent to requiring that the boundary response of component α be identical to the adjacent boundary response of component β. The actual enforcement of displacement or velocity constraints is achieved with a locator matrix [E] that consists only of zeroes and ones. The matrix [E] selects and orders interface degrees of freedom in $\underset{\sim}{X}(t)$ for each component so that

$$([E]\underset{\sim}{X}(t))_{\alpha} - ([E]\underset{\sim}{X}(t))_{\beta} = 0 \tag{6.5}$$

completely defines compatibility between α and β. An additional constraint is that the forces exerted on substructure α by substructure β must be equal and opposite to forces exerted on β and α.

Howsman [12] and Hale [11] achieve a systematic implementation of these constraints by using a variational principal. The details are quite lengthy, but a noteworthy consequence of the variational formulation is that the adjoint, or co-state, equations corresponding to Eqs. (6.3A) and (6.3B) are considered in the theory.

$$-[A_{\alpha}]^{T}\dot{\underset{\sim}{Y}}_{\alpha}(t) + [B_{\alpha}]^{T}\underset{\sim}{Y}_{\alpha}(t) = \underset{\sim}{F}^{Y}_{\alpha}(t) \tag{6.6A}$$

$$-[A_{\beta}]^{T}\dot{\underset{\sim}{Y}}_{\beta}(t) + [B_{\beta}]^{T}\underset{\sim}{Y}_{\beta}(t) = \underset{\sim}{F}^{Y}_{\beta}(t) \tag{6.6B}$$

The feature of component mode synthesis that permits the formulation of a reduced-order system model is the introduction of Ritz vectors. Unlike most other methods, however, references [11] and [12]

suggest Ritz approximations for the standard differential equations, Eq. (6.3), and the adjoint differential equation, Eq. (6.6).

$$\underset{\sim}{X}(t) \cong \sum_{K=1}^{N_X} \underset{\sim}{\psi}_{XK} \Gamma_{XK}(t) = [\underset{\sim}{\psi}_X] \underset{\sim}{\Gamma}_X(t) \tag{6.7A}$$

$$\underset{\sim}{Y}(t) \cong \sum_{K=1}^{N_Y} \underset{\sim}{\psi}_{YK} \Gamma_{YK}(t) = [\underset{\sim}{\psi}_Y] \underset{\sim}{\Gamma}_Y(t) \tag{6.7B}$$

The vectors $\underset{\sim}{\Gamma}_X(t)$ and $\underset{\sim}{\Gamma}_Y(t)$ are $N_X \times 1$ and $N_Y \times 1$. Equations (6.7A) and (6.7B) represent reductions in order when N_X and N_Y are chosen such that

$$N_X << N_C \tag{6.8A}$$

$$N_Y << N_C \tag{6.8B}$$

where N_C is the number of degrees of freedom for a component.

The fact that not all coordinates in the collective set $\underset{\sim}{\Gamma}_{XS}(t) = \{\Gamma_{X\alpha}(t), \Gamma_{X\beta}(t)\}$ are independent becomes apparent when the Ritz approximation, Eq. (6.7A) is substituted into Eq. (6.5).

$$([E][\underset{\sim}{\psi}_X]\underset{\sim}{\Gamma}_X(t))_\alpha - ([E][\underset{\sim}{\psi}_X]\underset{\sim}{\Gamma}_X(t))_\beta = 0 \tag{6.9}$$

If N_D is the number of displacement and velocity constraints in Eq. (6.9), then N_D of the coordinates in $\underset{\sim}{\Gamma}_{XS}(t)$ are redundant. The over-abundance of coordinates is remedied by requiring the user to select $N_\alpha + N_\beta - N_D$ independent coordinates from $\underset{\sim}{\Gamma}_{XS}(t)$. The set of coordinates $\underset{\sim}{\Gamma}_{XS}(t)$ is then expressible as a combination of the

independent coordinate vector $\underset{\sim}{\Gamma}_{XI}(t)$ of length $N_\alpha + N_\beta - N_D$.

$$\underset{\sim}{\Gamma}_{XS}(t) = \begin{bmatrix} \underset{\sim}{\Gamma}_{XI}(t) \\ \underset{\sim}{\Gamma}_{XD}(t) \end{bmatrix} = [C_X]\underset{\sim}{\Gamma}_{XI}(t) \tag{6.10}$$

The N_D-vector $\underset{\sim}{\Gamma}_{XD}(t)$ represents the dependent coordinates in $\underset{\sim}{\Gamma}_{XS}(t)$. The form of the $(N_\alpha + N_\beta) \times (N_\alpha + N_\beta - N_D)$ matrix $[C_X]$ in Eq. (6.10) is derived to be

$$[C_X] = \begin{bmatrix} [I] \\ -([E][\underset{\sim}{\psi}_X])_D^{-1}([E][\underset{\sim}{\psi}_X])_I \end{bmatrix} \tag{6.11}$$

A completely analogous argument may be used to define a similar matrix $[C_Y]$ corresponding to redundant coordinates in $\underset{\sim}{\Gamma}_{YS}(t)$.

With the transformations defined in Eqs. (6.7A), (6.7B) and (6.11), the variational formulation suggested in [12] yields the final reduced order system model.

$$[A_s]\dot{\underset{\sim}{\Gamma}}_{XI}(t) + [B_S]\underset{\sim}{\Gamma}_{XI}(t) = \underset{\sim}{F}_S(t) \tag{6.12}$$

where

$$[A_S] = [C_Y]^T \begin{bmatrix} [\underset{\sim}{\psi}_Y]_\alpha^T & 0 \\ 0 & [\underset{\sim}{\psi}_Y]_\beta^T \end{bmatrix} \begin{bmatrix} [A_\alpha] & 0 \\ 0 & [A_\beta] \end{bmatrix} \begin{bmatrix} [\underset{\sim}{\psi}_X]_\alpha & \\ & [\underset{\sim}{\psi}_X]_\beta \end{bmatrix} [C_X] \tag{6.13A}$$

$$[B_S] = [C_Y]^T \begin{bmatrix} [\underset{\sim}{\psi}_Y]_\alpha & 0 \\ 0 & [\underset{\sim}{\psi}_Y]_\beta \end{bmatrix} \begin{bmatrix} [B_\alpha] & 0 \\ 0 & [B_\beta] \end{bmatrix} \begin{bmatrix} [\underset{\sim}{\psi}_X]_\alpha & \\ & [\underset{\sim}{\psi}_X]_\beta \end{bmatrix} [C_X] \tag{6.13B}$$

$$F_S(t) = [C_Y]^T \begin{vmatrix} [\psi_Y]_\alpha & 0 \\ 0 & [\psi_Y]_\beta \end{vmatrix} \begin{vmatrix} F_\alpha(t) \\ F_\beta(t) \end{vmatrix} \tag{6.13C}$$

As in any Ritz approximation, the accuracy of the reduced-order model of Eq. (6.12) depends upon the selection of Ritz vectors in $[\psi_Y]$ and $[\psi_X]$ in Eqs. (6.13A), (6.13B) and (6.13C).

6.3 Analytical Ritz Vectors

Two types of Ritz vectors are used in the component mode synthesis method described in section (6.2). These are the so-called free-interface substructure modes and attachment modes. Strictly speaking, Eqs. (6.7A) and (6.7B) suggest that two different sets of Ritz vectors must be specified for each component. However, references [11] and [12] advocate choosing the sets to be identical to save computational costs.

$$\psi_X = \psi_Y \tag{6.14}$$

Free-interface substructure modes are quite common and are calculated from the eigenproblem for each component α and β. The columns of the matrices $[\psi_X]$ and $[\psi_Y]$ corresponding to substructure modes are denoted as X_r in Eq. (6.15).

$$\{\lambda_r[A] + [B]\}X_r = 0 \tag{6.15}$$

Implicit in Eq. (6.15) is that the substructure boundaries are free to displace. If the component eigenproblems are of sufficiently low order, it may be feasible to calculate $[\psi_X]$ and $[\psi_Y]$ separately. In this case,

the column vectors of $[\psi_Y]$ corresponding to substructure modes are derived from Y_r in the left eigenproblem

$$\{\lambda_r[A]^T + [B]^T\}Y_r = 0 \tag{6.16}$$

In their most fundamental form, the attachment modes may be defined as the displacement shapes resulting from a statically applied unit force at a single degree of freedom. Reference [12] generalizes this definition somewhat by expressing the attachment modes in a state vector form. The generalized pseudostatic response of the components α and β is of the form

$$[B]X = F \tag{6.17}$$

The attachment modes in the state vector formulation are then the set of Ritz vectors $[\psi_A]$ that satisfy

$$[\psi_A] = [B]^{-1}\begin{bmatrix} 0 \\ [I_A] \end{bmatrix} \tag{6.18}$$

$[I_A]$ is an identity matrix defining unit forces at several displacement degrees of freedom. From Eq. (6.18) it is obvious that standard attachment modes are simply columns of $[B]^{-1}$.

When a set of Ritz vectors is composed of both substructure modes, Eqs. (6.15) or (6.16), and attachment modes, Eqs. (6.18), some redundancy results. The standard attachment modes may be expressed as a linear combination of the substructure modes. If K is the number of substructure modes kept as Ritz vectors and N_C is the number of component degrees of freedom,

$$[B]^{-1} = \sum_{r=1}^{K} \frac{X_r Y_r^T}{-\lambda_r} + \sum_{r=K+1}^{2N_c} \frac{X_r Y_r^T}{-\lambda_r} \tag{6.19}$$

provides an explanation of attachment modes, or columns of $[B]^{-1}$, in terms of substructure modes. It is implicitly assumed in Eq. (6.19) that the product $a_r = Y_r^T [A] X_r$ is normalized to unity. The rightmost term in Eq. (6.19) represents the contribution to the attachment modes of higher substructure modes that are not retained in the Ritz basis.

A modification of standard attachment modes has been designed to represent the effects of the discarded higher modes. These "residual attachment modes" may be written

$$[\psi_{RA}] = \sum_{r=K+1}^{2N} \frac{X_r Y}{-\lambda_r} \tag{6.20A}$$

or

$$[\psi_{RA}] = [B]^{-1} - \sum_{r=1}^{K} \frac{X_r Y_r}{-\lambda_r} \tag{6.20B}$$

It is important to note that the residual attachment modes may be calculated from (6.20B) without explicit knowledge of the deleted modes, X_r and Y_r for i = K + 1 to $2N_C$.

6.4 Experimental Ritz Vectors

Experimental analogs of the analytical free interface substructure modes in Eq. (6.15) have already been derived in Chapter 2. Right eigenvectors of order $2N_C$ for each component may be

approximated from the experimental reduced model eigenvectors of order $2M_C \times 1$.

$$\underset{\sim}{X}_r = [\Psi_R]\hat{\underset{\sim}{X}}_r \tag{6.21}$$

The transformation $[\Psi_R]$ is $2N_c \times 2M_C$, in this case.

A derivation of experimental standard attachment modes can be carried out by considering the pseudostatic response of the reduced experimental model.

$$[\hat{B}]\underset{\sim}{\Gamma} = \hat{\underset{\sim}{F}} = \begin{bmatrix} [\hat{D}] \\ [0] \end{bmatrix} \underset{\sim}{p} \tag{6.22}$$

The elements of $[\hat{B}]$ have been completely defined in the solution of the least squares problem in Eq. (2.24). Assuming the inverse of $[\hat{B}]$ exists, the pseudostatic response of the reduced system to unit forces at N_p exciter locations is given in Eq. (6.23).

$$[\underset{\sim}{\Gamma}_1 \underset{\sim}{\Gamma}_2 \cdots \underset{\sim}{\Gamma}_{N_p}] = [\hat{B}]^{-1} \begin{bmatrix} [\hat{D}] \\ [0] \end{bmatrix} \tag{6.23}$$

Approximations of the standard attachment modes for the original system can be reconstructed from Eq. (6.23).

$$[\underset{\sim}{\psi}_A] \approx [\Psi_R]\,[\underset{\sim}{\Gamma}_1 \underset{\sim}{\Gamma}_2 \cdots \underset{\sim}{\Gamma}_{N_p}] = [\Psi_R][\hat{B}]^{-1} \begin{bmatrix} [\hat{D}] \\ [0] \end{bmatrix} \tag{6.24}$$

Residual attachment modes may also be estimated from the pseudostatic response of the reduced system. The vector $\underset{\sim}{\Gamma}$ in Eq. (6.22) may be expressed as a superposition of the reduced right eigenvectors.

$$\underset{\sim}{\Gamma} = \sum_{r=1}^{K} \hat{\underset{\sim}{X}}_r q_r + \sum_{r=k+1}^{2M_c} \hat{\underset{\sim}{X}}_r q_r \tag{6.25}$$

The first summation in Eq. (6.25) includes modes estimated accurately in the extraction procedure. These modes are analogous to the kept modes in Eq. (6.19). The last summation in Eq. (6.25) represents discarded, higher frequency modes.

When Eq. (6.25) is substituted into Eq. (6.22) and premultiplied by the rth left eigenvector $\hat{\underset{\sim}{Y}}_r$, all terms vanish except

$$\hat{\underset{\sim}{Y}}_r^T [\hat{B}] \hat{\underset{\sim}{X}}_r q_r = \hat{\underset{\sim}{Y}}_r^T \hat{\underset{\sim}{F}} \tag{6.26A}$$

or

$$\hat{b}_r q_r = \hat{\underset{\sim}{Y}}_r^T \hat{\underset{\sim}{F}} \tag{6.26B}$$

With the introduction of $\hat{b}_r = -\lambda_r \hat{a}_r$ from Eq. (3.30), Eq. (6.26) can be recombined with Eq. (6.25).

$$\underset{\sim}{\Gamma} = \sum_{r=1}^{K} \frac{\hat{\underset{\sim}{X}}_r \hat{\underset{\sim}{Y}}_r^T \hat{\underset{\sim}{F}}}{-\hat{\lambda}_r \hat{a}_r} + \sum_{r=K+1}^{2M_c} \frac{\hat{\underset{\sim}{X}}_r \hat{\underset{\sim}{Y}}_r^T \hat{\underset{\sim}{F}}}{-\hat{\lambda}_r \hat{a}_r} \tag{6.27}$$

As in Eq. (6.19), the left and right terms in Eq. (6.27) can be identified as the contribution to the reduced pseudostatic response of kept and deleted reduced system modes. Residual attachment modes of the original system relative to N_p exciter locations can be approximated from Eq. (6.27) by introducing the estimate to $\underset{\sim}{\Gamma}$ in Eq. (6.23) and the reconstructing transformation $[\psi_R]$

$$[\psi_{RA}] \cong [\psi_R] [\hat{B}]^{-1} - \sum_{r=1}^{K} \frac{\hat{\underset{\sim}{X}}_r \hat{\underset{\sim}{Y}}_r^T}{-\hat{\lambda}_r \hat{a}_r} \begin{bmatrix} [\hat{D}] \\ \underset{\sim}{0} \end{bmatrix} \tag{6.28}$$

Chapter 7

VERIFICATION OF THE METHOD

This chapter outlines two studies conducted to validate the parameter extraction method introduced in this thesis. Two characteristics of the approach are emphasized in the verification process. Section (7.1) focuses upon the convergence and stability properties of the technique in the presence of noise when either of the transformations discussed in Chapter 4 is utilized. In section (7.2), the performance of the method in resolving closely-spaced modes is compared to other methods.

7.1 Stability Example

In the first example, the 8-DOF finite element model of the beam-rotor assembly shown in Figure (7.1) is considered. As apparent in the illustration, the model makes provision for discrete damping at all degrees of freedom. Moreover, the two rotors in the assembly lead to Coriolis damping, which manifests itself in a skew-symmetric damping matrix. As a result, the system modes are complex. The system mass, damping and stiffness matrices are listed in Tables (7.1), (7.2) and (7.3).

Using the aforementioned analytic model, simulated experimental response spectra have been generated and later analyzed by the parameter estimation method. By comparing the resulting approximate modal parameters to those obtained directly from the analytic model, the accuracy of the technique may be gauged.

Actual measurements all contain some level of noise. Inasmuch as it is desirable to simulate physically realizable systems, random noise has been added to the simulated signals in proportion to the RMS response signal level. If $\{\ddot{x}_j(w_1)\ddot{x}_j(w_2) \ldots\}$ represents the acceleration spectrum of the jth degree of freedom, then

$$\ddot{x}_j^{RMS} = \sqrt{\frac{\Sigma \ddot{x}_j(w_1)\ddot{x}_j(w_2)}{N_w}} \tag{7.1}$$

is the RMS response signal level used in noise calibration. Specifically, the noise added to the Lth frequency point of the response spectrum for the jth degree of freedom is calculated from

$$N_j(w_L) = S\ddot{x}_j^{RMS} \, W \frac{\ddot{x}_j(w_L)}{\sqrt{N_w \ddot{x}_j(w_L)\ddot{x}_j(w_L)}} \tag{7.2}$$

where

$N_j(w_L)$ = the complex noise added to $\ddot{x}_j(w_L)$
S = a user input noise-to-signal ratio
W = a random, uniform (0,1) weighting factor
N_w = number of frequency points in the spectrum

An extensive set of runs has been carried out for the analytic model. The parameters comprising the mass, stiffness and damping matrices in Tables (7.1), (7.2) and (7.3) have been selected such that two moderately damped complex modes reside in the frequency range from 256 to 512 rad/sec.

	DAMPED FREQUENCY	DAMPING RATIO	
MODE 1	309.2 (RAD/SEC)	.08231	(7.3A)
MODE 2	420.6 (RAD/SEC)	.05444	(7.3B)

In the simulation, 512 frequency points are used, with a frequency resolution of $\Delta w = 0.3516$ rad/sec.

Table (7.4) depicts in matrix form the particular cases considered in the verification. Each entry in the matrix denotes the actual number of runs executed for a particular set of conditions.

MODEL ORDER	NOISE-TO-SIGNAL RATIO					
	0%	2%	4%	6%	8%	10%
8	10	10	10	10	10	10
7	10	10	10	10	10	10
6	10	10	10	10	10	10

TABLE (7.4)

Each test condition is executed 10 times because random excitation has been simulated in all studies. As shown in the table, the noise-to-signal ratio is increased from 0% to 10% in 2% increments for models comprised of 6th to 8th order matrices. Because two reduction methods have been suggested in Chapter 4, the entire matrix in Table (7.4) is repeated for both the independent coordinate and the principal component transformations.

Figures (7.2) through (7.9) summarize the error incurred in estimating the modal parameters for the various noise levels, model orders and transformation types. Each point in the figures represents the median of the 10 runs conducted for every case in Table (7.4). The noise-to-signal ratio described in Eq. (7.2) is plotted along the abscissa in all the graphs. The normalized error for a particular type of modal parameter is charted along each ordinate. Equations (7.4A),

(7.4B) and (7.4C) define the normalized error computed for damped frequencies, decay rates and the ith complex mode, respectively.

$$E_w = \left| \frac{\hat{w}_d - w_d}{w_d} \right| \tag{7.4A}$$

$$E_\sigma = \left| \frac{\hat{\sigma} - \sigma}{\sigma} \right| \tag{7.4B}$$

$$E_{\underset{\sim}{X}} = \left| \frac{\overline{(\hat{\underset{\sim}{X}}_i - \underset{\sim}{X}_i)}^T (\hat{\underset{\sim}{X}}_i - \underset{\sim}{X}_i)}{\bar{\underset{\sim}{X}}_i^T \underset{\sim}{X}_i} \right| \tag{7.4C}$$

In Eqs. (7.4A) through (7.4B), the quantities $\hat{w}_d$, $\hat{\sigma}$, $\hat{\underset{\sim}{X}}$ are the approximated damped frequency, decay rate and complex modes, while w_d, σ and $\underset{\sim}{X}$ are exact values calculated from the analytic model.

As suggested in previous studies [3], estimates of the damped frequency are the most accurate of the approximated modal parameters. Figures (7.2) through (7.5) depict the damped frequency normalized error at different noise levels for the modes at 309 rad/sec and 420 rad/sec. Each line on the graphs indicates the error level for a specific model order. For example, Figure (7.2) shows that the 6th and 7th order model have less error in the frequency estimates than the full order model for high noise levels.

Both independent coordinate and principal component transformations yield excellent frequency estimates. Inspection of Figures (7.2) through (7.5) shows that the damped frequency at 309 rad/sec has been estimated using an independent coordinate transformation with a median error less than 0.48% for all noise levels. Likewise, the

principal component approximation of the same mode has a median error less than 0.80%. Similar results hold for the mode at 420 rad/sec. When an independent coordinate reduction is employed, the 420 rad/sec damped frequency is estimated with a maximum median error of 0.40%. A median error less than 1.8% is achieved when approximating the same mode using a principal component transformation.

In the current analysis, approximations to the decay rate and mode shape for the 309 rad/sec mode are typical of the method's performance for all estimated modes. Figures (7.6) and (7.7) indicate that the maximum median error in decay rate is from 12% to 15% for both the independent coordinate and principal component reduction strategies. However, in both cases the error in decay rate is considerably less over much of the noise range considered. When independent coordinates are used in Figure (7.6), the decay rate actually improves in accuracy (4% to 6%) as the noise level is increased. All but three data points reside below the 7% median error level in Figure (7.7), where principal components have been used.

Figures (7.8) and (7.9) depict the normalized modal vector error incurred in estimating the 309 rad/sec mode. In the case in which independent coordinates have been selected, the maximum median error is roughly 2.80% and occurs at the 10% noise-to-signal level. The principal component study illustrated in Figure (7.9) has a maximum normalized modal error 8.0%. Again, the error in estimating the modes is much less over the majority of the investigated noise range.

In reviewing the performance of the technique, both transformation methods yield accurate parameter estimates, despite the

introduction of relatively high noise levels. Damped frequency approximations are particularly good, though the examples suggest that the principal component estimates typically approach the exact values from above. The use of an independent coordinate reduction has generated slightly more precise approximations than those obtained using principal components. This comparison emphasizes an important attribute of the principal component reduction strategy; the accuracy of the approach depends upon the accuracy of the estimated variance matrix in Eq. (4.19). Moreover, the precision of the variance matrix is reliant upon the sample record size N_w in Eq. (4.20). [4]

In the test cases executed in this chapter, a record length of 512 points has been used. Preliminary studies with even fewer frequency points, $N_w = 256$, have resulted in still higher error levels for the principal component reduction strategy. Evidently, a tradeoff exists. The principal component reduction method is desirable in that it can provide an estimate of the number of active modes in a frequency range. Yet, for a small sample size, the accuracy of the method may suffer.

7.2 Mode Resolution Example

Section (7.1) has given an example in which the current method is shown to be stable in the presence of significant random noise levels. While such a demonstration is certainly necessary, a major motivation for the use of any multi-shaker method is its ability to extract closely-spaced modes. [13] The remainder of this section compares the performance of the current method to that of other multiple-DOF techniques in resolving closely-spaced modes.

Towards this goal, an experimental modal analysis of the dual beams shown in Figure (7.10) has been carried out using the current technique, the Polyreference method, and the complex exponential method. The beams in Figure (7.10) are designed such that the natural frequencies of the system occur in closely-spaced pairs. Uncorrelated, random excitation has been applied simultaneously at stations 4Z+ and 5Z+, and acceleration responses have been measured at locations 1Z+ to 8Z+. A frequency range of 0 to 256 Hz and a sampling rate of 1024 samples/second have been used in data acquisition. All pertinent dimensions and location labels are shown in Figure (7.10), and Figures (7.11A) and (7.11B) show photographs of the actual experimental setup. Tables (7.5A) and (7.5B) list the equipment and channel configuration used in the experiment. A synopsis of the data acquisition conditions is provided in Table (7.6).

The only difference between the data acquisition conditions used in the current method and that used in the Polyreference or complex exponential techniques is the ensemble size. As evidenced in Table (7.6), 10 records of time history data are collected in the runs using the Polyreference and complex exponential algorithms. Only one record is collected for use in the method introduced in this thesis. The primary reason for the additional records in the Polyreference and complex exponential methods is that they utilize frequency response functions in their estimation processes. To achieve FRF's sufficiently smooth for parameter extraction, 10 records are used. Because the current method uses raw spectra, only 1 record of time history data is required.

Tables (7.7A) and (7.7B) summarize the damped frequency and damping level for two of the modes estimated in the analyses. Four runs using an independent coordinate reduction strategy are listed, as well as four runs using a principal component reduction scheme. Similarly, the results of two runs are tabulated for each of the Polyreference and complex exponential techniques.

The first table gives the approximations of the lower of the two highly coupled modes. The damped frequencies obtained in the Polyreference and complex exponential techniques vary from 118.4 to 120.5 hz. When independent coordinates have been generated, the damped frequency estimates range from 118.6 to 119.9 hz, in close agreement with the other methods. Two of the estimates achieved with the use of principal components are 120.2 and 120.9 hz, again in close correlation with the other methods. As noted in the analytical example problem, the damped frequencies for the principal component reduction strategy seem to approach the actual values from above.

As might be expected from other studies [3], the damping values for all techniques are more varied. In the Polyreference and complex exponential algorithms, damping values range from .00255 to .02595. Similarly, the damping levels estimated using independent coordinate and principal component transformations range from .00300 to .00535, and from .00143 to .0101, respectively.

In Table (7.7B), approximations to the higher of the two closely spaced modes are listed. Correlation between the Polyreference method and the current technique is again quite good. The complex exponential algorithm, however, yields uniformly high

estimates of the damped frequency and damping level. This tendency may be attributed in part to the relatively modest number of frames in the ensemble. Other runs using the complex exponential method with fewer frames of data have shown even higher estimates of the modal parameters.

As a final observation, both Householder's technique and singular value decomposition have performed comparably in terms of accuracy and stability in these experimental example runs. The singular value decomposition algorithm has required slightly more user input to execute. In practical analyses, extremely small computed singular values may degrade accuracy and should be set equal to zero. Selection of the threshold value below which to zero singular values seems to require a significant amount of intuition. For this reason, Householder's method can be especially well suited for those unfamiliar with least squares solution procedures.

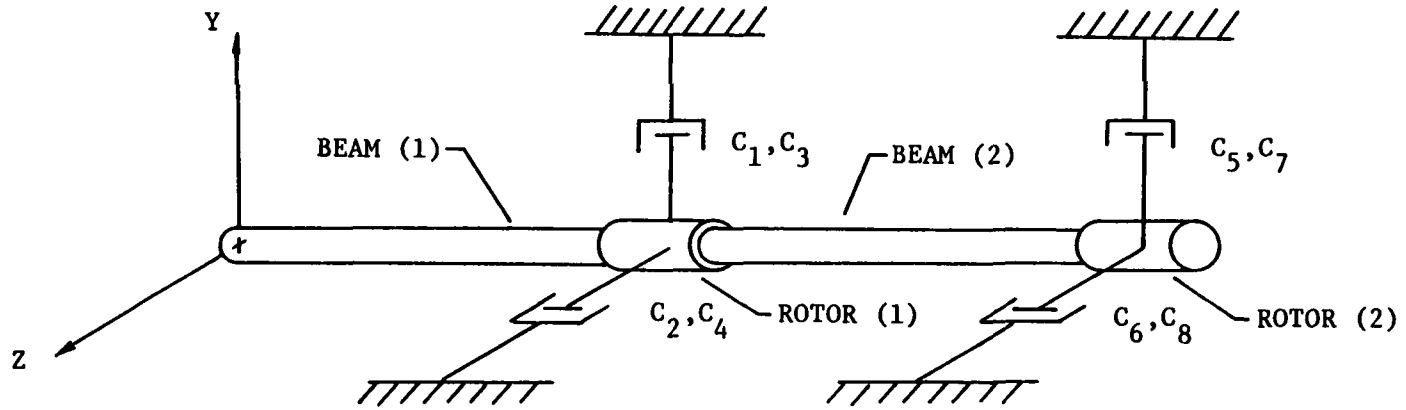

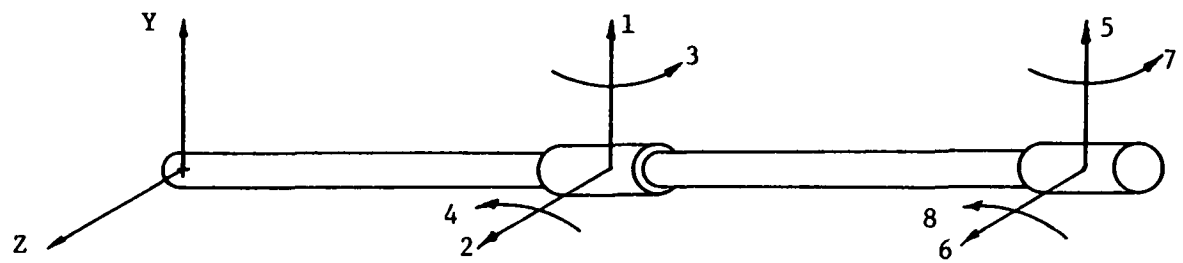

8-DOF ANALYTICAL MODEL

FIGURE (7.1)

$$[M] = \begin{bmatrix} m_{11} & 0 & 0 & m_{14} & m_{15} & 0 & 0 & m_{18} \\ & m_{22} & m_{23} & 0 & 0 & m_{26} & m_{27} & 0 \\ & & m_{33} & 0 & 0 & m_{36} & m_{37} & 0 \\ & & & m_{44} & m_{45} & 0 & 0 & m_{48} \\ & & & & m_{55} & 0 & 0 & m_{58} \\ & & & & & m_{66} & m_{67} & 0 \\ & & & & & & m_{77} & 0 \\ \text{— Symmetric —} & & & & & & & m_{88} \end{bmatrix}$$

$$m_{11} = m_{22} = \frac{156}{420}(\rho_1 A_1 L_1 + \rho_2 A_2 L_2) + m_{1C} + m_{1R}$$

$$m_{33} = m_{44} = \frac{4}{420}(\rho_1 A_1 L_1^3 + \rho_2 A_2 L_2^3) + J_1$$

$$m_{55} = m_{66} = \frac{156}{420}(\rho_2 A_2 L_2) + m_{2C} + m_{2R}$$

$$m_{77} = m_{88} = \frac{4}{420}(\rho_2 A_2 L_2^3) + J_2$$

$$m_{14} = -m_{23} = \frac{-22}{420}(\rho_1 A_1 L_1^2 - \rho_2 A_2 L_2^2)$$

$$m_{15} = -m_{26} = \frac{54}{420}(\rho_2 A_2 L_2)$$

$$m_{18} = -m_{27} = \frac{-13}{420}(\rho_2 A_2 L_2^2)$$

$$m_{36} = -m_{45} = m_{18}$$

$$m_{37} = -m_{48} = \frac{-3}{420}(\rho_2 A_2 L_2^3)$$

$$m_{58} = -m_{67} = \frac{22}{420}(\rho_2 A_2 L_2^2)$$

ρ_1, ρ_2 - Beam Density

A_1, A_2 - Beam Cross-Sectional Area

L_1, L_2 - Beam Length

m_{1C}, m_{2C} - Mass of Rotor Casing

m_{1R}, m_{2R} - Mass of Rotor

I_1, I_2 - Transverse Inertia of Rotor

J_1, J_2 - Axial Inertia of Rotor

TABLE (7.1)

$$[K] = \begin{bmatrix} k_{11} & 0 & 0 & k_{14} & k_{15} & 0 & 0 & k_{18} \\ & k_{22} & k_{23} & 0 & 0 & k_{26} & k_{27} & 0 \\ & & k_{33} & 0 & 0 & k_{36} & k_{37} & 0 \\ & & & k_{44} & k_{45} & 0 & 0 & k_{48} \\ & & & & k_{55} & 0 & 0 & k_{58} \\ & & & & & k_{66} & k_{45} & 0 \\ & & & & & & k_{77} & 0 \\ & & \text{— Symmetric —} & & & & & k_{88} \end{bmatrix}$$

$$k_{11} = \frac{12E_1I_{1Z}}{L_1^3} + \frac{12E_2I_{2Z}}{L_2^3} \qquad k_{14} = \frac{6E_2I_{2Z}}{L_2^2} + \frac{6E_1J_{1Z}}{L_1^2}$$

$$k_{22} = \frac{12E_1J_{1Y}}{L_1^3} + \frac{12E_2I_{2Y}}{L_2^3} \qquad k_{23} = \frac{6E_1J_{1Y}}{L_1^2} - \frac{6E_2I_{2Y}}{L_2^2}$$

$$k_{33} = \frac{4E_1I_{1Y}}{L_1} + \frac{4E_2I_{2Y}}{L_2} \qquad k_{15} = \frac{-12E_2I_{2Z}}{L_2^3}$$

$$k_{44} = \frac{4E_1I_{1Z}}{L_1} + \frac{4E_2J_{2Z}}{L_2} \qquad k_{26} = \frac{-12E_2I_{2Y}}{L_2^3}$$

$$k_{55} = \frac{12E_2I_{2Z}}{L_2^3} \qquad k_{18} = \frac{6E_2I_{2Z}}{L_2^2}$$

$$k_{66} = \frac{12E_2I_{2Y}}{L_2^3} \qquad k_{27} = \frac{-6E_2I_{2Y}}{L_2^2}$$

$$k_{77} = \frac{4E_2I_{2Y}}{L_2} \qquad k_{36} = -k_{27}$$

$$k_{88} = \frac{4E_2I_{2Z}}{L_2} \qquad k_{45} = -k_{18}$$

$$k_{58} = -k_{18} \qquad k_{37} = \frac{2E_2I_{2Y}}{L_2}$$

$$k_{67} = -k_{27} \qquad k_{48} = \frac{2E_2I_{2Z}}{L_2}$$

J_{1Z}, J_{2Z}, J_{1Y}, J_{2Y} - Inertia About Z-Axis, Inertia About X-Axis

L_1, L_2 - Beam Length

E_1, E_2 - Elastic Modulus

TABLE (7.2)

$$[C] = \begin{bmatrix} c_1 & & & & & & & \\ & c_2 & & & & & & \\ & & c_3 & (I_1-J_1)\Omega_1 & & & & \\ & & -(I_1-J_1)\Omega_1 & c_4 & & & & \\ & & & & c_5 & & & \\ & & & & & c_6 & & \\ & & & & & & c_7 & (I_2-J_2)\Omega_2 \\ & & & & & & -(I_2-J_2)\Omega_2 & c_8 \end{bmatrix}$$

$c_1 \cdots c_8$	-	Discrete Damping
I_1, I_2	-	Transverse Inertia of Rotor
J_1, J_2	-	Axial Inertia of Rotor
Ω_1, Ω_2	-	Rotor Angular Frequency

TABLE (7.3)

FIGURE (7.2)

309 RAD/SEC
DAMPED FREQUENCY NORMALIZED ERROR
-vs-
NOISE-TO-SIGNAL RATIO

INDEPENDENT COORDINATE TRANSFORMATION

o - 8th order model
+ - 7th order model
△ - 6th order model

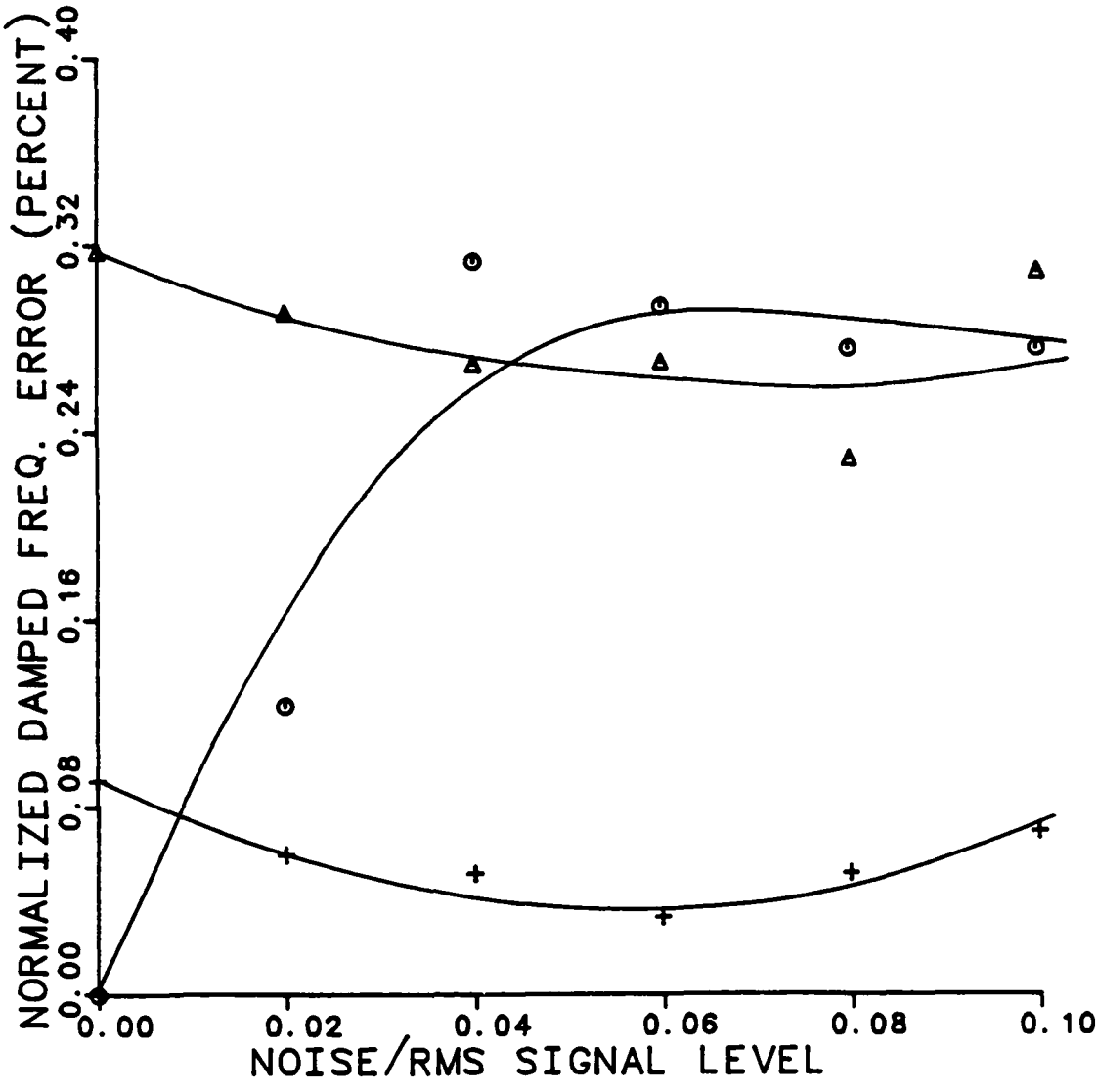

FIGURE (7.3)

309 RAD/SEC
DAMPED FREQUENCY NORMALIZED ERROR
-vs-
NOISE-TO-SIGNAL RATIO

PRINCIPAL COMPONENT TRANSFORMATION

o - 8th order model
+ - 7th order model
△ - 6th order model

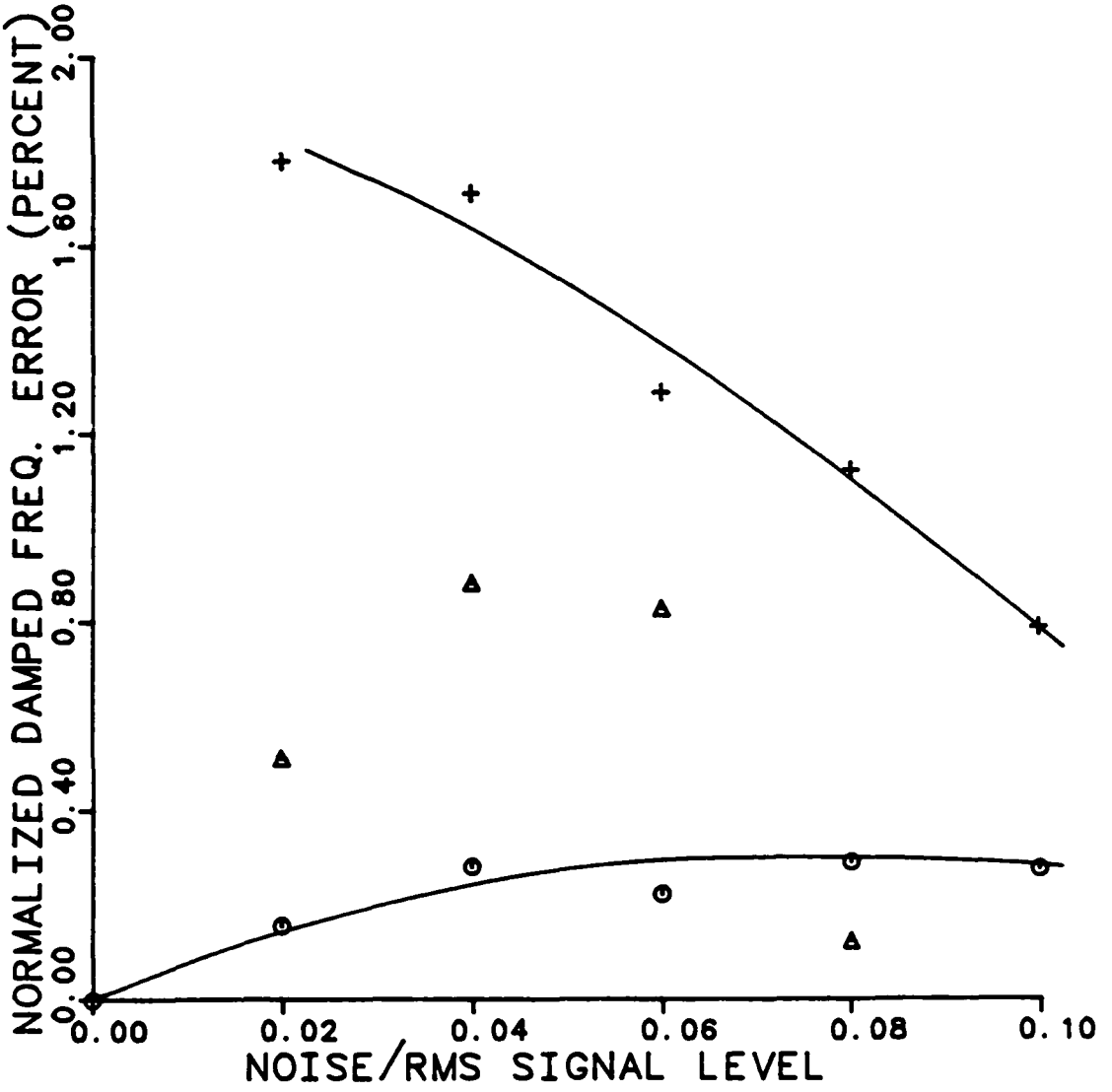

FIGURE (7.4)

420 RAD/SEC
DAMPED FREQUENCY NORMALIZED ERROR
-vs-
NOISE-TO-SIGNAL RATIO

INDEPENDENT COORDINATE TRANSFORMATION

o - 8th order model
+ - 7th order model
△ - 6th order model

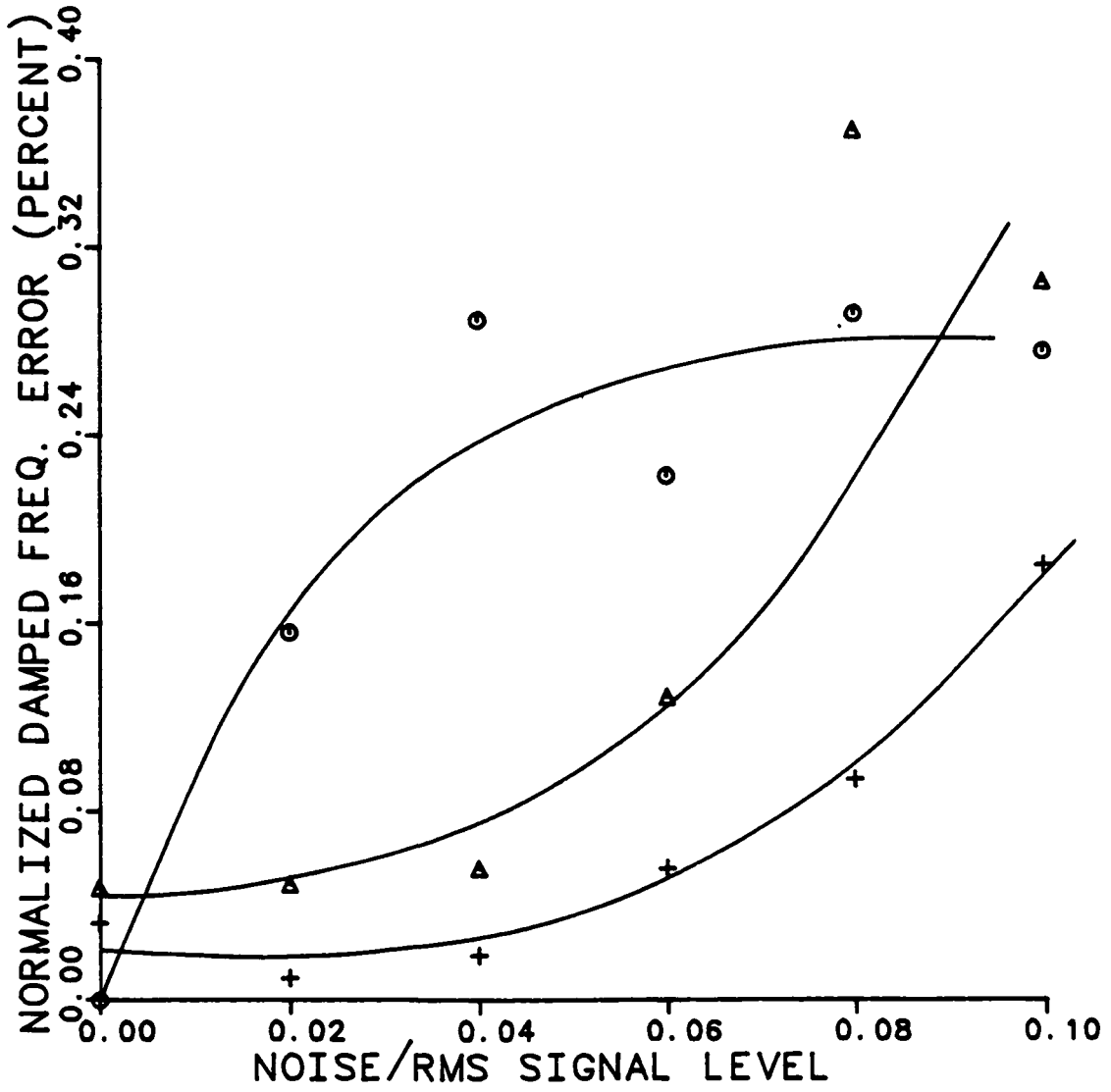

FIGURE (7.5)

309 RAD/SEC
DAMPED FREQUENCY NORMALIZED ERROR
-vs-
NOISE-TO-SIGNAL RATIO

PRINCIPAL COMPONENT TRANSFORMATION

o - 8th order model
+ - 7th order model
△ - 6th order model

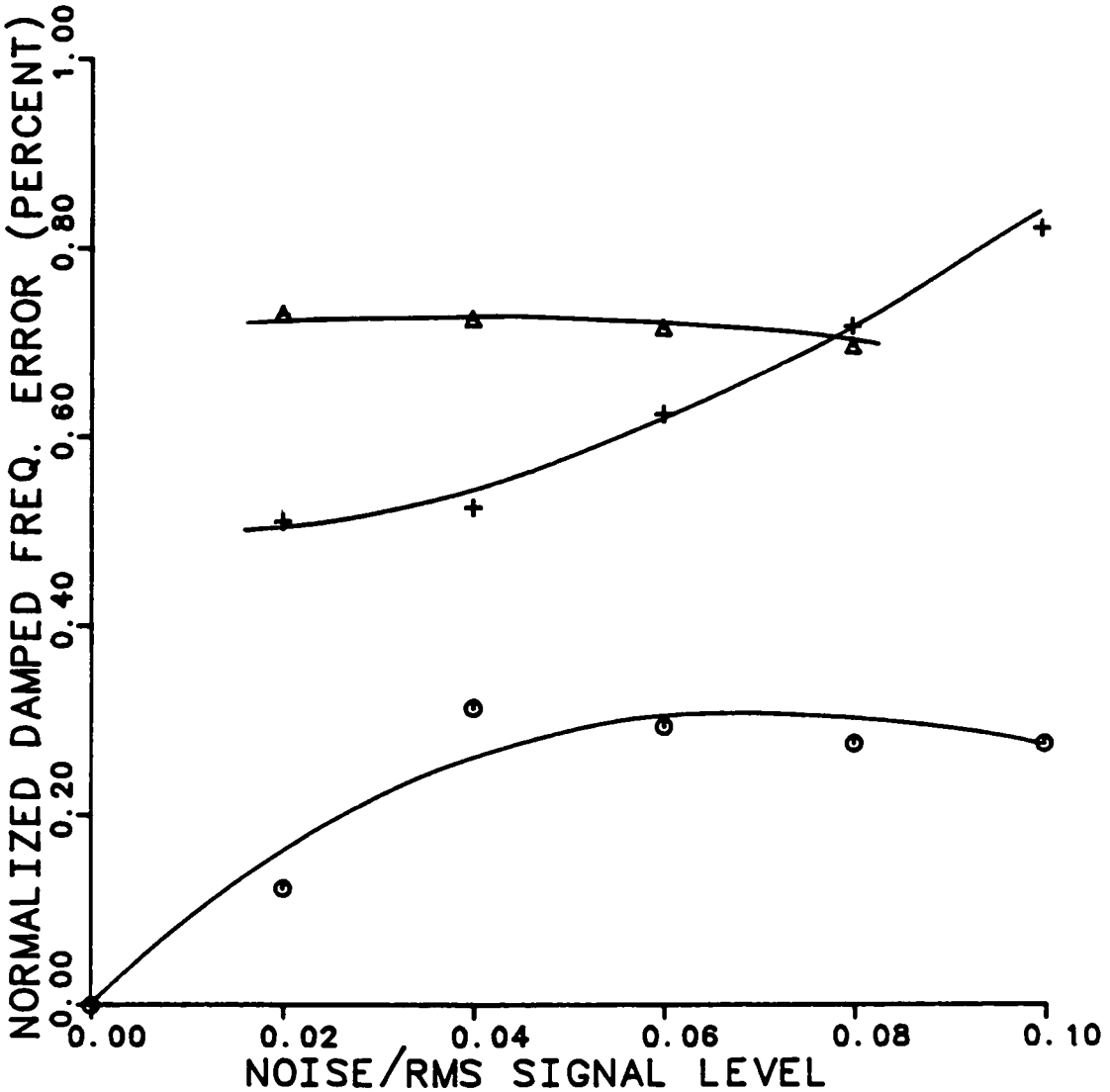

FIGURE (7.6)

309 RAD/SEC
DECAY RATE NORMALIZED ERROR
-vs-
NOISE-TO-SIGNAL RATIO

INDEPENDENT COORDINATE TRANSFORMATION

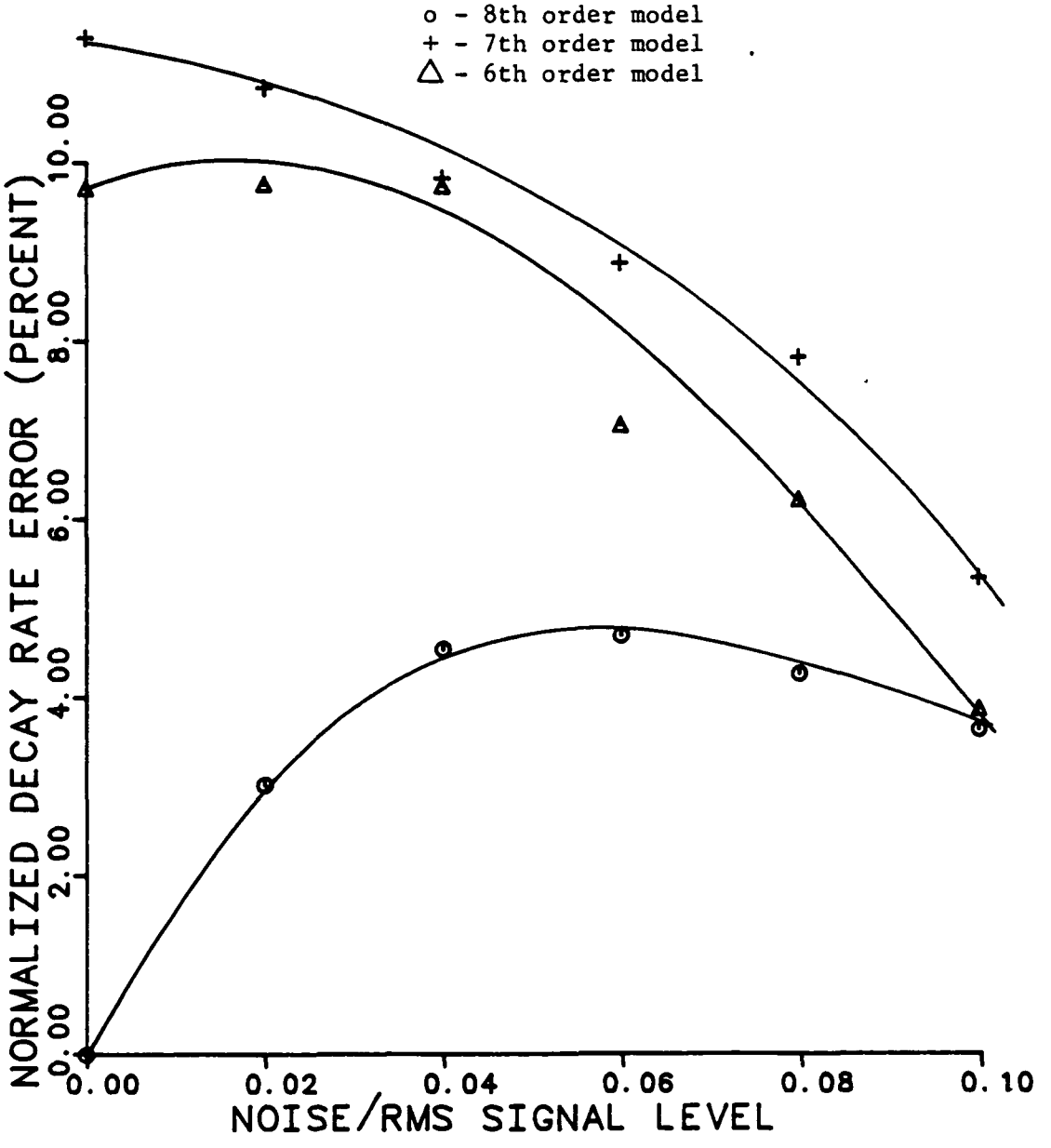

FIGURE (7.7)

420 RAD/SEC
DECAY RATE NORMALIZED ERROR
-vs-
NOISE-TO-SIGNAL RATIO

PRINCIPAL COMPONENT TRANSFORMATION

o - 8th order model
+ - 7th order model
△ - 6th order model

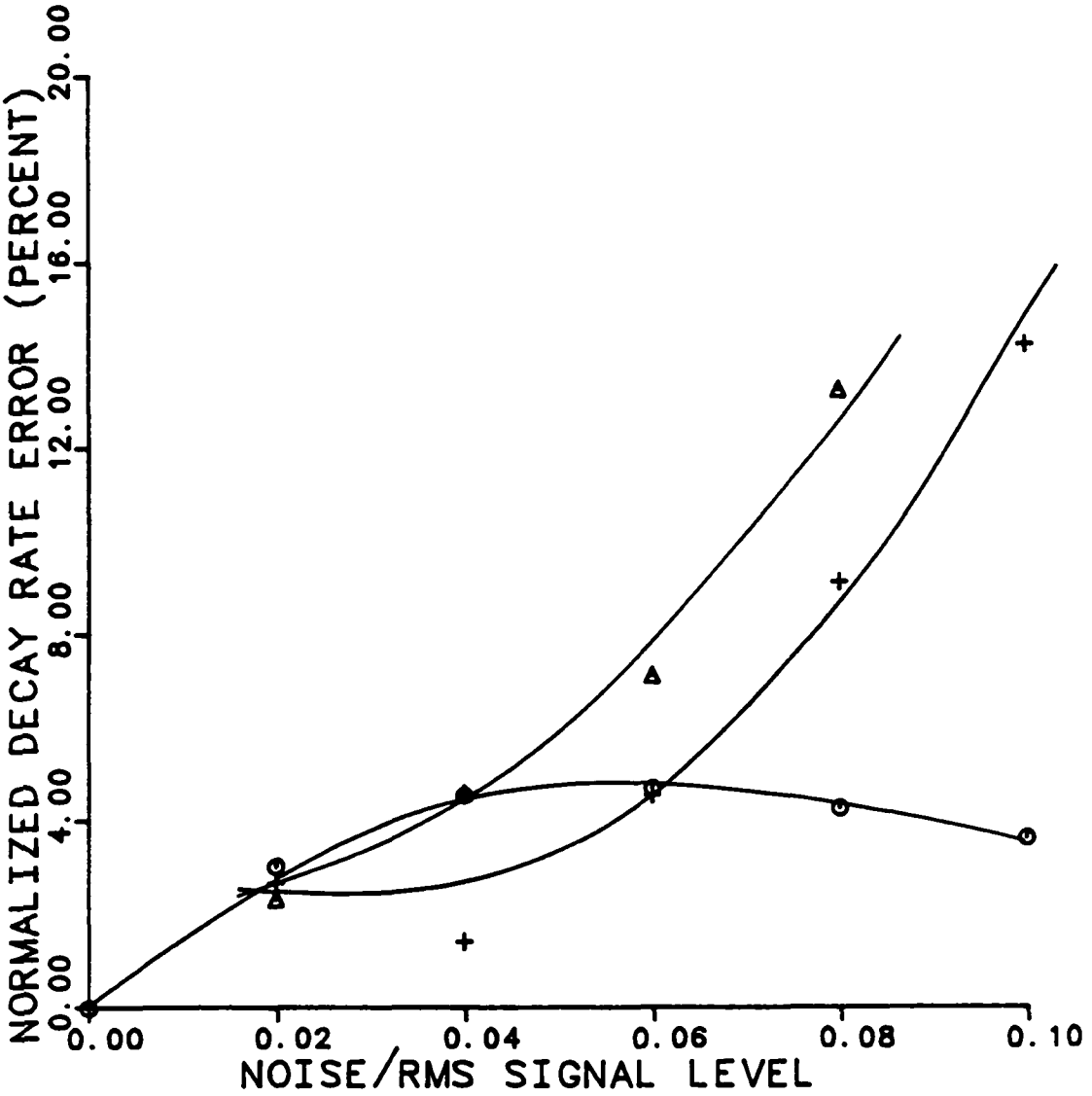

FIGURE (7.8)

309 RAD/SEC
MODAL NORMALIZED ERROR
-vs-
NOISE-TO-SIGNAL RATIO

INDEPENDENT COORDINATE TRANSFORMATION

o - 8th order model
+ - 7th order model
△ - 6th order model

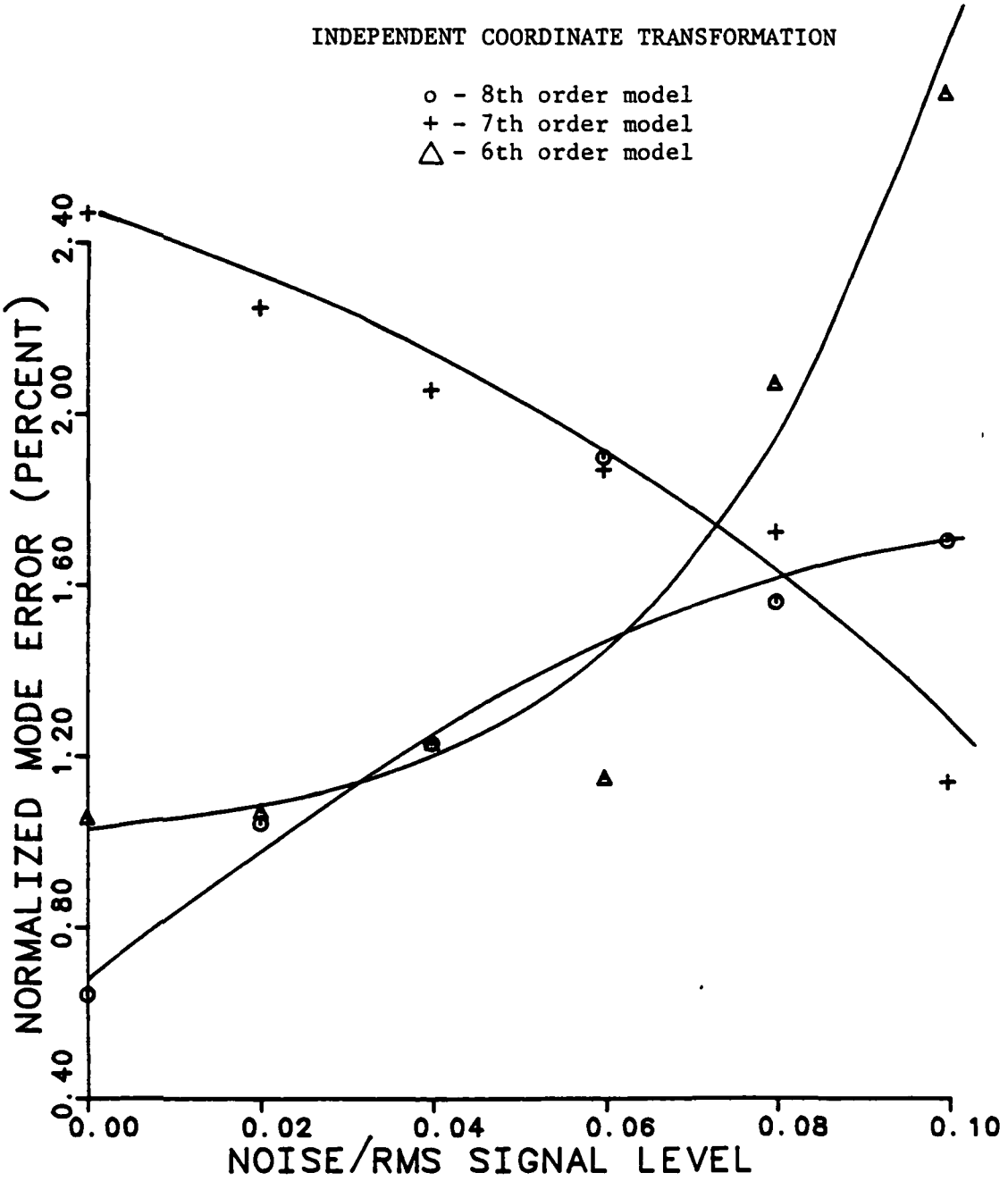

FIGURE (7.9)

309 RAD/SEC
MODAL NORMALIZED ERROR
-vs-
NOISE-TO-SIGNAL RATIO

PRINCIPAL COMPONENT TRANSFORMATION

o - 8th order model
+ - 7th order model
△ - 6th order model

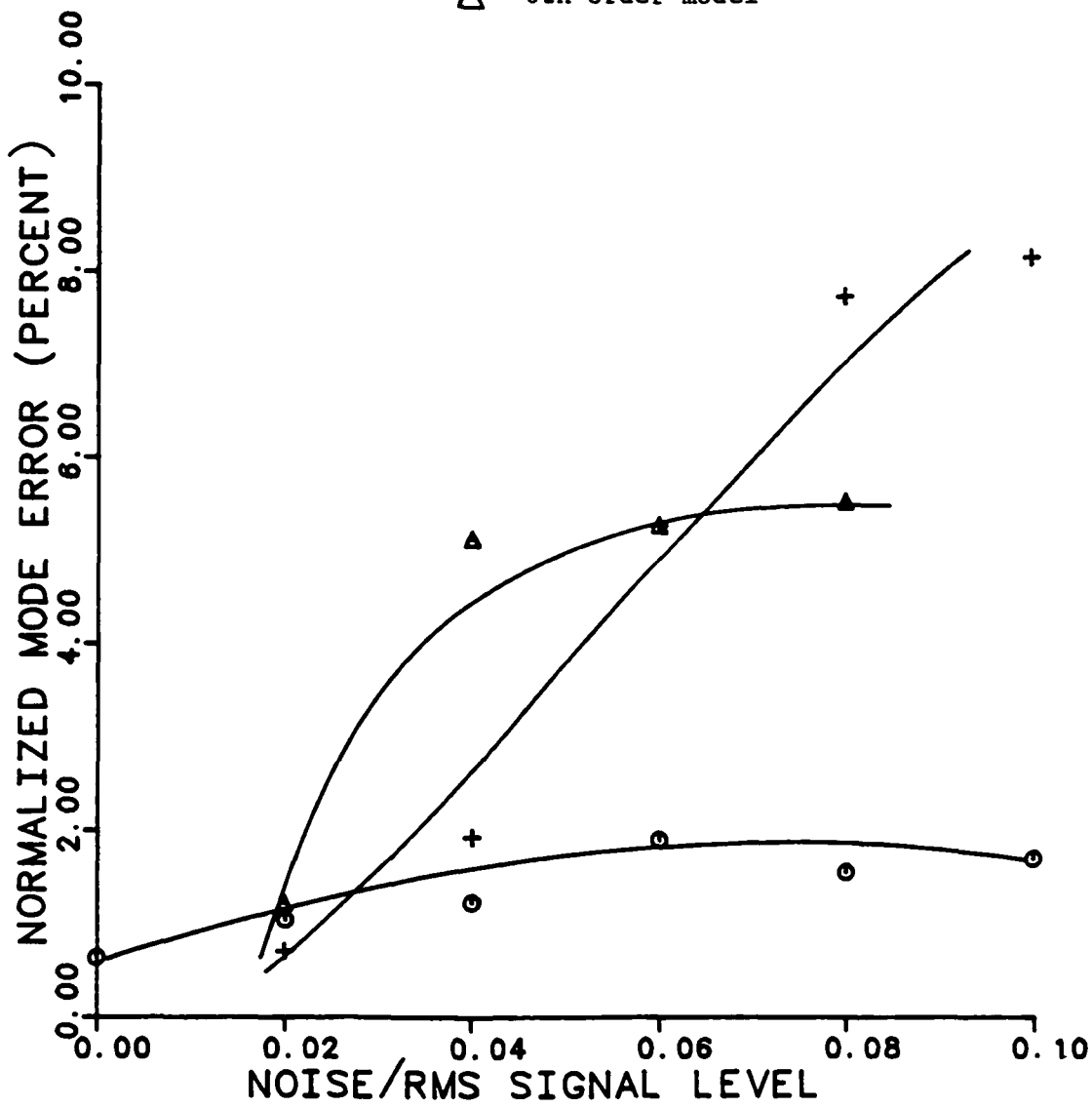

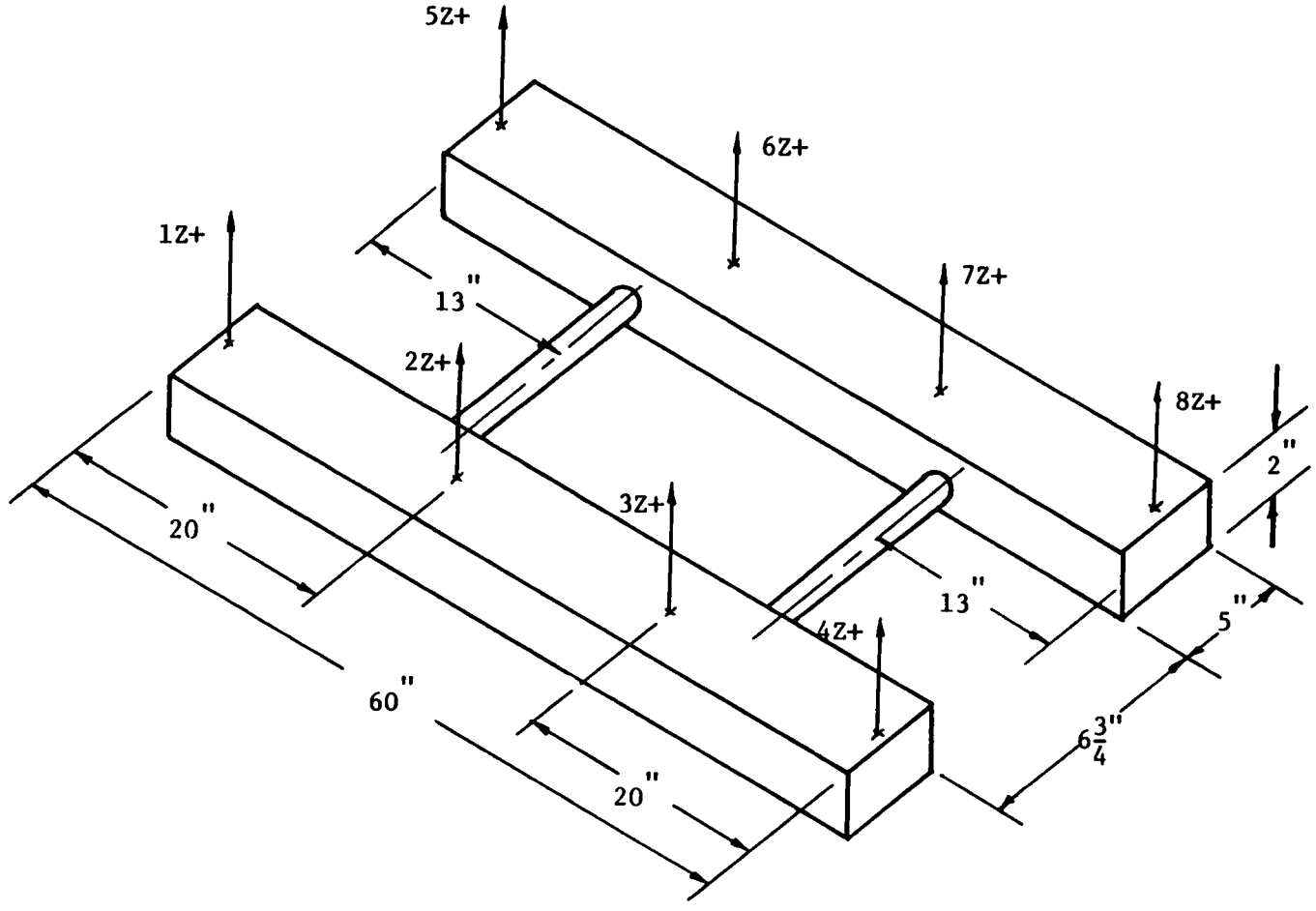

DUAL BEAM DIMENSIONS

FIGURE (7.10)

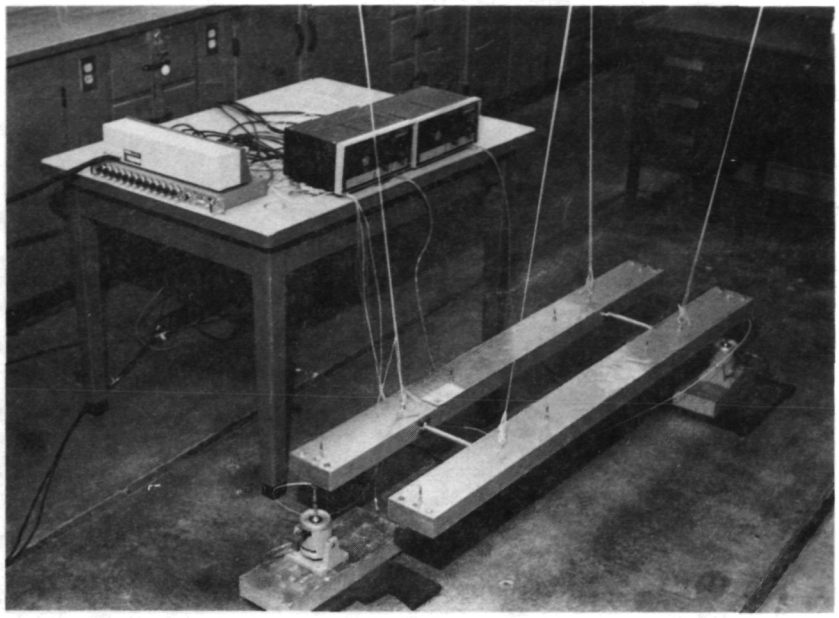

FIGURE (7.11A) Dual beams with shakers at $4Z^+$ and $5Z^+$.

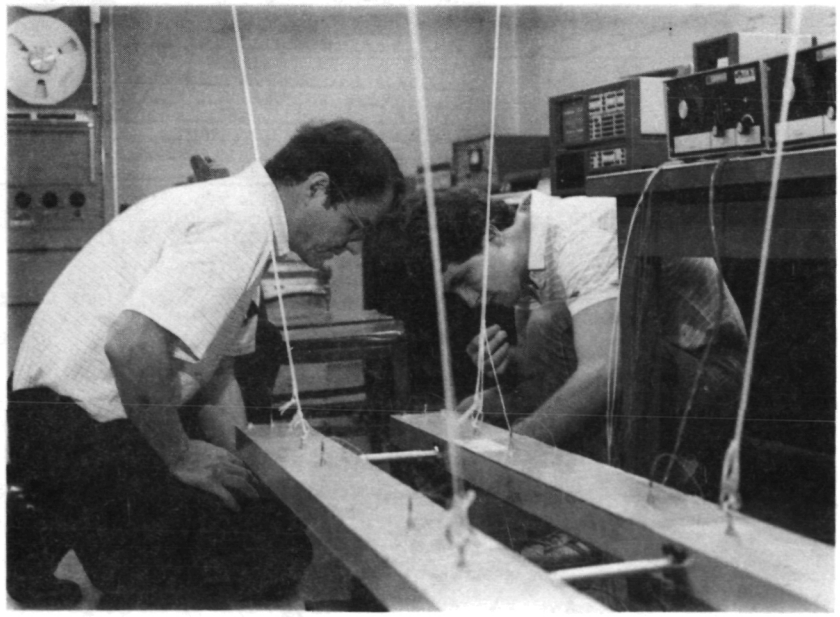

FIGURE (7.11B) Closeup of dual beams, Ling amplifiers, GENRAD 2515 and HP recorder.

TABLE (7.5A)

DATA ACQUISITION EQUIPMENT

DESCRIPTION:

GENRAD 2515 Computer Aided Test System 1

GENRAD 16-Channel Expansion 1

PCB Signal Conditioner, Model 483A17 1

LING 200 Series Vibrator 2

LING Power Amplifier, Model TPO 25 2

PCB Accelerometers, 303A SERIES 8

PCB Force Transducers,208B SERIES 2

HP 3900 Tape Recorder 1

TABLE (7.5B)

CHANNEL CONFIGURATION

CHANNEL NO.	SIGNAL TYPE	COOR-DINATE	VOLTAGE RANGE	CALIBRATION SCALE		ACCELEROMETER SERIAL NO.
1	Force	4Z+	-8.0, 8.0	1.85185E-3	lb/mv	SN 3967
2	Force	5Z+	-8.0, 8.0	1.84502E-3	lb/mv	SN 3965
3	Accel.	1Z+	-.125, .125	0.10061	g/mv	SN 5915
4	Accel.	2Z+	-.125, .125	0.10204	g/mv	SN 4743
5	Accel.	3Z+	-.125, .125	9.31099E-2	g/mv	SN 4344
6	Accel.	4Z+	-.125, .125	0.10152	g/mv	SN 5937
7	Accel.	5Z+	-.125, .125	9.78474E-2	g/mv	SN 5916
8	Accel.	6Z+	-.125, .125	9.31099E-2	g/mv	SN 4520
9	Accel.	7Z+	-.125, .125	0.10741	g/mv	SN 4613
10	Accel.	8Z+	-.125, .125			

TABLE (7.6)

DATA ACQUISITION CONDITIONS

PROPOSED METHOD:

Sampling Frequency ($f = 1/\Delta t$)	1024
Frequency Range	0-256 HZ
Excitation	Random
References	2, uncorrelated
Responses	8
Ensemble Size	1
Record Size	2048 PTS

POLYREFERENCE/COMPLEX EXPONENTIAL:

Sampling Frequency ($f = 1/\ t$)	1024
Frequency Range	0-256 HZ
Excitation	Random/Hanning Window
References	2, uncorrelated
Responses	8
Ensemble Size	10
Record Size	2048 PTS

	Model order 7		Model order 6		Model order 5		Model order 4	
	freq.	damping	freq.	damping	freq.	damping	freq.	damping
INDEPENDENT COORDINATES	119.9	.00300	119.2	.00429	118.7	.00535	118.6	.00337
PRINCIPAL COMPONENTS	120.2	.00143	121.7	.01010	120.9	.00718	122.0	.00327

	RUN (1)		RUN (2)	
	freq.	damping	freq.	damping
POLYREFERENCE	119.8	.01599	120.5	.00863

	RUN (1)		RUN (2)	
	freq.	damping	freq.	damping
COMPLEX EXPONENTIAL	118.4	.02595	118.582	.00255

TABLE (7.7A)

	Model order 7		Model order 6		Model order 5		Model order 4	
	freq.	damping	freq.	damping	freq.	damping	freq.	damping
INDEPENDENT COORDINATES	123.7	.00233	125.4	.01230	123.0	.01790	124.7	.00770
PRINCIPAL COMPONENTS	124.4	.00719	124.6	.00820	123.4	.00200	124.9	.00971

	RUN (1)		RUN (2)	
	freq.	damping	freq.	damping
POLYREFERENCE	123.1	.00521	123.7	.00679

	RUN (1)		RUN (2)	
	freq.	damping	freq.	damping
COMPLEX EXPONENTIAL	128.9	.05424	127.8	.01378

TABLE (7.7B)

Chapter 8

CONCLUSIONS

A modal parameter estimation procedure applicable to linear, time-invariant systems has been presented in this thesis. In the technique, multiple non-coherent input excitations may be applied to the structure. A consistent set of modal parameters is generated in the algorithm.

The technique is formulated such that no assumptions concerning the damping matrix [C] are made. Despite relatively high noise levels, accurate damped frequencies, decay rates and complex modes have been calculated in Chapter 7 for a system with both skew-symmetric and non-proportional damping terms.

As with Blair's modification of the SFD algorithm, the current method has been shown to accurately resolve closely spaced modes. An experimental comparison has shown that the parameters obtained in the current method are comparable to those achieved with the Polyreference and complex exponential algorithms.

Two solution procedures noted for their stability, the singular value decomposition technique and Householder's method, have been evaluated in conjunction with numerous verification runs of the method. In practical experimental analyses, both methods have been shown to be accurate and stable. Householder's method has been found more favorable due to its faster execution time and ease of use.

Since many practical modal analyses involve numerous measurement locations, two different transformations are investigated to reduce the size of the actual problem to be solved. Both approaches attempt to minimize the amount of required user interaction. The independent coordinate reduction method is shown to be more accurate for a small sample size in several example runs. The principal component reduction algorithm can provide an estimate of the number of modes active in a given frequency range.

Further development is needed in several areas related to this thesis. As an example, the procedures suggested in Chapter 6 to calculate standard and residual attachment modes from experimental data should undergo numerical study. Another potential application of the method might investigate the use of the experimental reduced systems matrices directly in a substructure coupling procedure.

Modifications of the method itself may also be considered. Some of the statistical methods mentioned in [16] could be incorporated into the model reduction process. Another improvement might be to modify the least squares problem for the reduced system matrices in Eq. (2.24) such that frequency response functions are used instead of spectra. In the present form, increasing the size of the experimental samples to achieve greater accuracy necessarily creates a larger least squares problem for the system matrices. If frequency response functions are used, they could be smoothed by increasing the number of averages, or ensemble size, used in their acquisition. The least squares problem for reduced system matrices could then use frequency

response functions smoothed by averaging, instead of increasing the number of frequency points in the raw spectra.

Finally, additional work on the development of accurate and easily calculable modal confidence factors for the present method should be pursued. A procedure that automatically rejects the most obvious spurious modes would be most desirable.

REFERENCES

1. Allemang, R.J., "Experimental Modal Analysis," Modal Testing and Model Refinement, ASME, New York, 1983.

2. Bathe, K.J., and Wilson, E.L., Numerical Methods in Finite Element Analysis, Prentice-Hall, Inc., Englewood Cliffs, New Jersey, 1976.

3. Blair, M., and Craig, R.R., "Digital Multi-Shaker Modal Testing," Report to NASA Marshall Space Flight Center, Contract No. NAS8-33980, The University of Texas at Austin, Austin, Texas, 1983.

4. Brillinger, D., Time Series : Data Analysis and Theory, Holden-Day, San Francisco, 1981.

5. Brown, D.L., Allemang, R.J., and Mergeay, M., "Parameter Estimation Techniques for Modal Analysis," SAE Paper No. 790221, SAE Transactions, Vol. 88, Sect. 1, 1979, pp. 828,846.

6. Chung, Y.T., "Application and Experimental Determination of Substructure Coupling for Damped Structural Systems," Ph.D. Dissertation, The University of Texas at Austin, Austin, Texas, 1982.

7. Coppolino, R.N., "A Simultaneous Frequency Domain Technique for Estimation of Modal Parameters from Measured Data," SAE Paper No. 811046, SAE Transactions, Vol. 10, Sect. 5, 1981, pp. 1005,1046.

8. Craig, R.R., Jr., Structural Dynamics : An Introduction to Computer Methods, John Wiley and Sons, Inc., New York, 1981.

9. Golub, G.H., and Van Loan, C.F., Matrix Computations, The Johns Hopkins University Press, Baltimore, Maryland, 1983.

10. Greenberg, M.D., Foundations of Applied Mathematics, Prentice-Hall, Inc., Englewood Cliffs, New Jersey, 1978.

11. Hale, A.L., "On Substructure Synthesis and Its Iterative Improvement for Large Nonconservative Vibratory Systems," AIAA Paper No. 82-0772, Proc. of the 23rd Structures, Structural Dynamics and Materials Conference, New Orleans, May, 1982, pp. 582-593.

12. Howsman, T.G., "A Substructure Coupling Procedure Applicable to General Linear Time-Invariant Dynamic Systems," Master's Thesis, The University of Texas at Austin, Austin, Texas, 1983.

13. Juang, Jer-nan, and Pappa, R.S., "An Eigensolution Realization Algorithm for Modal Parameter Identification and Model Reduction," Paper Presented at the NASA/JPL Workshop on Identification and Control of Flexible Space Structures, San Diego, Calif., June 4-6, 1984.

14. Lawson, C.L., and Hanson, R.J., Solving Least Square Problems, Prentice-Hall, Inc., Englewood Cliffs, New Jersey, 1974.

15. Leuridan, J.M., Brown, D.L., and Allemang, R.J., "Direct System Parameter Identification of Mechanical Structures with Application to Modal Analysis," AIAA Paper No. 82-0767, Proc. of the 23rd Structures, Structural Dynamics and Materials Conference, New Orleans, 1982.

16. Mardia, K.V., Kent, J.T., and Bibby, J.M., Multivariate Analysis, Academic Press, London, 1979.

17. Martinez, D.R., Carne, T.G., Gregory, D.L., and Miller, K.A., "Combined Experimental/Analytical Modelling Using Component Mode Synthesis," Sandia Report No. 1889, Sandia National Laboratories, Albuquerque, New Mexico, 1984.

18. Martinez, D.R., and Gregory, D.L., "A Comparison of Free Component Mode Synthesis Techniques Using MSC/NASTRAN," Sandia Report No. 0025, Sandia National Laboratories, Albuquerque, New Mexico, 1984.

19. Meirovitch, L., Analytical Methods in Vibration, The MacMillan Company, New York, 1967.

20. MODAL ANALYSIS 8.0 Users Manual, "Modal Analysis Theory," Chapter 6, GE CAE International Inc., Milford, Ohio, 1983.

21. Ralston, A., and Rabinowitz, P., A First Course in Numerical Analysis, McGraw-Hill Book Company, New York, 1978.

22. Ramsey, K.A., "Effective Measurements for Structural Dynamics Testing," Sound and Vibration, Vol. 9, No. 11, Nov., 1975.

23. Richardson, M., "Modal Analysis Using Digital Test Systems," Hewlett Packard Publication 02-5952-7032, Oct., 1975.

24. Rubin, S., "Improved Component-Mode Representation for Structural Dynamic Analysis," AIAA Journal, Vol. 13, No. 8, Aug., 1975, pp. 995-1006.